Article

Landscape of helper and regulatory antitumour CD4$^+$ T cells in melanoma

https://doi.org/10.1038/s41586-022-04682-5

Received: 23 July 2021

Accepted: 23 March 2022

Published online: 4 May 2022

Check for updates

Giacomo Oliveira[1,2]✉, Kari Stromhaug[1], Nicoletta Cieri[1], J. Bryan Iorgulescu[1,2,3], Susan Klaeger[4], Jacquelyn O. Wolff[5], Suzanna Rachimi[4], Vipheaviny Chea[6], Kate Krause[7], Samuel S. Freeman[2,4], Wandi Zhang[1], Shuqiang Li[4,6], David A. Braun[1,2,4,8], Donna Neuberg[9], Steven A. Carr[4], Kenneth J. Livak[1,6], Dennie T. Frederick[4,10], Edward F. Fritsch[1,4], Megan Wind-Rotolo[11], Nir Hacohen[2,4,10], Moshe Sade-Feldman[4,10], Charles H. Yoon[1,12], Derin B. Keskin[1,6,13,14], Patrick A. Ott[1,2,4,15], Scott J. Rodig[3,15], Genevieve M. Boland[2,4,7] & Catherine J. Wu[1,2,4,15]✉

Within the tumour microenvironment, CD4$^+$ T cells can promote or suppress antitumour responses through the recognition of antigens presented by human leukocyte antigen (HLA) class II molecules[1,2], but how cancers co-opt these physiologic processes to achieve immune evasion remains incompletely understood. Here we performed in-depth analysis of the phenotype and tumour specificity of CD4$^+$ T cells infiltrating human melanoma specimens, finding that exhausted cytotoxic CD4$^+$ T cells could be directly induced by melanoma cells through recognition of HLA class II-restricted neoantigens, and also HLA class I-restricted tumour-associated antigens. CD4$^+$ T regulatory (T_{Reg}) cells could be indirectly elicited through presentation of tumour antigens via antigen-presenting cells. Notably, numerous tumour-reactive CD4$^+$ T_{Reg} clones were stimulated directly by HLA class II-positive melanoma and demonstrated specificity for melanoma neoantigens. This phenomenon was observed in the presence of an extremely high tumour neoantigen load, which we confirmed to be associated with HLA class II positivity through the analysis of 116 melanoma specimens. Our data reveal the landscape of infiltrating CD4$^+$ T cells in melanoma and point to the presentation of HLA class II-restricted neoantigens and direct engagement of immunosuppressive CD4$^+$ T_{Reg} cells as a mechanism of immune evasion that is favoured in HLA class II-positive melanoma.

Antigen-specific CD4$^+$ T cells have a central role in adaptive immunity[1], since they can polarize immune responses as T helper cells, orchestrate humoral responses as T follicular helper (T_{FH}) cells, modulate the activity of effector cells as T_{Reg} cells, or directly kill targets as cytotoxic T cells[2]. Several studies have demonstrated the presence of CD4$^+$ tumour-infiltrating lymphocytes (TILs) in diverse cancers[3–7] and that they can have a role in determining the outcome of therapies[8,9]. Although CD4$^+$ TILs can be elicited though the interaction of T cell receptors (TCRs) with peptide–HLA class II complexes expressed on target cells[1,2], the mechanisms driving their activation within the tumour microenvironment (TME) remain unclear[10], especially since only a minority of tumours express HLA class II molecules at high levels[11,12]. Therefore, how CD4$^+$ TILs interact with tumour cells and the identity of the tumour antigens that can elicit cytotoxic or regulatory responses remain poorly understood.

Here we performed single-cell characterization of CD4$^+$ TILs from human melanomas with low or high expression of HLA class II and used TCR reconstruction to reveal the tumour specificity of CD4$^+$ TILs. By testing TCR reactivity against autologous patient-derived melanoma cell lines (pdMel-CLs) or antigen-presenting cells (APCs) loaded with tumour lysates, we assessed the capacity of CD4$^+$ TCRs to directly or indirectly recognize tumour cells. Our studies thus enabled the unambiguous linking of the phenotypes and antigen specificities of antitumour CD4$^+$ TILs.

Cell states of CD4$^+$ TIL TCR clonotypes

We profiled CD4$^+$ TILs in five tumour specimens collected prior to immune checkpoint blockade from four previously reported patients[13] (Pt-A, Pt-B, Pt-C and Pt-D) with stage III/IV melanoma (Supplementary Table 1). We characterized CD45$^-$ and CD45$^+$CD3$^+$ TIL fractions by high-throughput single-cell RNA sequencing (scRNA-seq) and single-cell TCR sequencing (scTCR-seq) coupled with detection of surface proteins (that is, cellular indexing of transcriptomes and epitopes by sequencing[14] (CITE-seq)) (Fig. 1a, Supplementary Table 2).

[1]Department of Medical Oncology, Dana-Farber Cancer Institute, Boston, MA, USA. [2]Harvard Medical School, Boston, MA, USA. [3]Department of Pathology, Brigham and Women's Hospital, Boston, MA, USA. [4]Broad Institute of MIT and Harvard, Cambridge, MA, USA. [5]Center for Immuno-Oncology, Dana-Farber Cancer Institute, Boston, MA, USA. [6]Translational Immunogenomics Laboratory, Dana-Farber Cancer Institute, Boston, MA, USA. [7]Department of surgery, Massachusetts General Hospital, Boston, MA, USA. [8]Center of Molecular and Cellular Oncology, Yale Cancer Center, Yale School of Medicine, New Haven, CT, USA. [9]Department of Data Science, Dana-Farber Cancer Institute, Boston, MA, USA. [10]Center for Cancer Research, Massachusetts General Hospital, Boston, MA, USA. [11]Bristol-Myers Squibb, Cambridge, MA, USA. [12]Division of Surgical Oncology, Brigham and Women's Hospital Boston, Boston, MA, USA. [13]Department of Computer Science, Metropolitan College, Boston University, Boston, MA, USA. [14]Department of Health Technology, Technical University of Denmark, Lyngby, Denmark. [15]Department of Medicine, Brigham and Women's Hospital, Boston, MA, USA. ✉e-mail: giacomo_oliveira@dfci.harvard.edu; cwu@partners.org

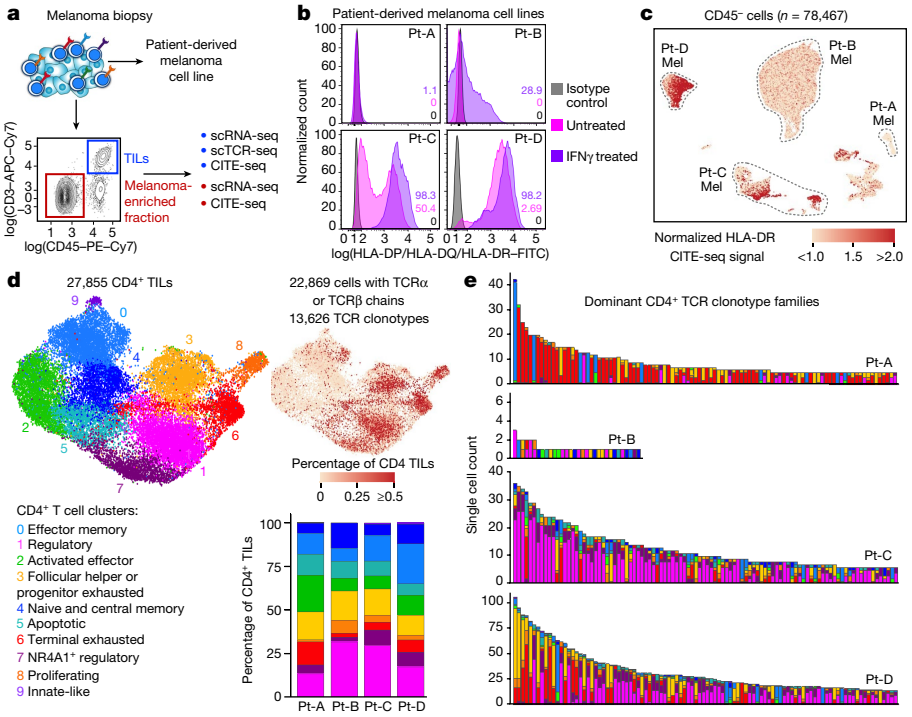

Fig. 1 | Melanoma HLA class II expression and phenotype of CD4⁺ TIL TCR clonotypes. a, Schematic of processing and single-cell sequencing analysis of melanoma samples. **b**, Flow cytometric assessment of HLA class II expression in 4 pdMel-CLs under basal culture conditions (magenta) or on exposure to IFNγ for 72 h (purple), compared with isotype control (grey). **c**, Uniform manifold approximation and projection (UMAP) of scRNA-seq data from tumour-enriched CD45⁻ cells isolated from melanomas from four patients. Clusters of patients' melanoma cells (Mel) were inferred on the basis of markers reported in Extended Data Fig. 1a–c. Colour indicates surface HLA-DR expression as determined by CITE-seq. **d**, UMAP of inferred cell states from scRNA-seq data of CD4⁺ TILs. Right, CD4⁺ TILs on the same UMAP, annotated for intra-patient TCR-clone frequency (defined by scTCR-seq). Bottom right, cluster frequencies among CD4⁺ TILs from the four patients. **e**, Cluster distribution of the top 100 CD4⁺ TCR clonotype families from melanomas from the four patients. Colours indicate cell states, as delineated in **d**.

PdMel-CLs that faithfully recapitulated the genomic and transcriptomic features of parental tumours were generated as described[13].

To evaluate whether melanomas could directly stimulate CD4⁺ TILs, we assessed expression of HLA class II in tumours. Flow cytometry analysis showed that HLA class II was not expressed in pdMel-CLs from Pt-A and Pt-B, and remained negative in Pt-A even under inflammatory conditions (with interferon-γ (IFNγ) treatment) (Fig. 1b). By contrast, pdMel-CLs from Pt-C and Pt-D showed evident baseline expression of HLA class II, which was confirmed in the parental primary tumours by scRNA-seq and CITE-seq (Fig. 1c, Extended Data Fig. 1a–f,). Immunohistochemistry (IHC) staining of primary specimens confirmed the expression of HLA class II in tumours (Extended Data Fig. 1g), which was maintained over time in biopsies serially collected from Pt-C. We also observed consistency and stability of HLA class II expression between pdMel-CLs and parental tumours in 8 pdMel-CLs generated from 17 independent treatment-naive melanomas and cultured without an inflammatory milieu (Extended Data Fig. 1h, i, Supplementary Table 3). Indeed, a subset of melanomas showed constitutive and stable presentation of surface HLA class II complexes.

To determine whether these disparate patterns of melanoma HLA class II expression were mirrored by diverse landscapes of CD4⁺ TILs, we analysed 27,855 CD4⁺ TILs characterized by scRNA-seq and CITE-seq[13] (Supplementary Table 4). The CD4⁺ TILs segregated into ten clusters (Fig. 1d, top, Extended Data Fig. 2a, Supplementary Table 5) based on the expression of T cell-related genes and enrichment of gene signatures from external single-cell datasets[4–6] (Extended Data Fig. 2b–e). This process (Supplementary Results) led us to define major CD4⁺ T cell phenotypes, such as naive T (T_N) and central memory T (T_{CM}), effector memory T (T_{EM}), activated effector T (T_{AE}) and terminally exhausted (T_{TE}) TILs and T_{FH} cells with features of progenitor exhausted (T_{PE}) TILs (T_{FH}/T_{PE})[15]. We further identified two T_{Reg} clusters, exhausted proliferating cells (T_{Prol}), apoptotic cells (T_{Ap}) and rare CD4⁺ cells with receptors of innate-like cells (T_{Inn}).

To assess the relationship between phenotype and TCR clonality, we used scTCR-seq to identify TCR αβ-chains from 22,869 cells that were grouped into 13,626 distinct CD4⁺ clonotypes (Extended Data Fig. 3a, Supplementary Table 4). Highly expanded clones were distributed among exhausted CD4⁺ TILs (T_{TE}, T_{FH}/T_{PE} and T_{Prol}; Fig. 1d, right), but also among T_{Reg} TILs, as confirmed by the skewing of TCR diversity in these clusters (Extended Data Fig. 3b). The cellular phenotypes within each expanded CD4⁺ TIL TCR clonotype were highly homogeneous (Extended Data Fig. 3c) and appeared to follow three distinct major patterns (Fig. 1e, Extended Data Fig. 3d): (1) the predominant acquisition of an exhausted phenotype (T_{Ex}), comprising T_{TE}, T_{FH}/T_{PE} and T_{Prol} cells; (2) the predominant acquisition of a non-exhausted memory phenotype (T_{NExM}), comprising T_N/T_{CM}, T_{EM} and T_{AE}; and (3) the acquisition of a T_{Reg} fate. This enabled the assignment of one of these three patterns to each expanded TCR clonotype as the dominant 'primary phenotype'. Notably, we observed that clonal expansion of CD4⁺ T_{Reg} TILs was far greater within the TME of the HLA class II-positive (HLA class II^{pos}) tumours from Pt-C and Pt-D (Fig. 1e).

Tumour-reactivity of CD4⁺ TIL TCRs

We sought to determine whether the TCR clonotypes from these diverse CD4⁺ phenotypic patterns were characterized by differences in the extent of tumour recognition. Given the marked expansion of T_{Reg} clonotypes in HLA class II^{pos} melanomas, we further hypothesized that such tumours could directly control the presentation of antigens to CD4⁺ TILs, thereby orchestrating the activation of both effector cells and potentially immunosuppressive T_{Reg} cells. From patients with high numbers of CD4⁺ TILs (Pt-A, Pt-C and Pt-D), we reconstructed 19 T_{NExM}

TCRs, 56 T_{Ex} TCRs (distributed across 18 T_{FH}/T_{PE} TCRs and 38 T_{TE}/T_{Prol} TCRs) and 56 T_{Reg} TCRs and expressed them in T cells from healthy donors (Methods). We determined tumour-specific reactivity on the basis of the upregulation of the activation molecule CD137[16], following co-culture of $CD4^+$ TCR-transduced cells with autologous pdMel-CLs that were either pretreated or not with IFNγ to induce HLA class II upregulation. In parallel, we also tested the TCRs against non-tumour controls—autologous peripheral blood mononuclear cells (PBMCs), B cells and Epstein–Barr virus (EBV)-immortalized lymphoblastoid cell lines (EBV-LCLs) (Extended Data Fig. 4a, b).

We found the T_{NExM} TCRs to be poorly tumour-reactive, since only one of the TCRs derived from Pt-D exhibited moderate recognition of autologous tumour (Fig. 2a); notably, three out of six T_{NExM} TCRs from Pt-A demonstrated viral reactivity, as shown by the specific recognition of EBV-infected targets. By contrast, the $CD4^+$ T_{Ex} compartment was enriched for antitumour specificities. T_{TE}/T_{Prol} phenotypes were the most enriched in tumour-specific reactivity across all 3 patients, with 32 out of 38 (84%) TCRs demonstrating tumour-specific activation. For T_{FH}/T_{PE} phenotypes, 5 out of 18 (28%) TCRs exhibited modest tumour recognition, exclusively in patients with HLA class II^{pos} melanoma (Pt-C and Pt-D). Strikingly, only in Pt-C and Pt-D, the T_{Reg} clusters were highly enriched for tumour-specific TCRs (28 out of 41 (68%) T_{Reg} TCRs). These data thus show that HLA class II^{pos} melanomas can directly engage and stimulate TCRs expressed by $CD4^+$ TILs with potential immunosuppressive capabilities (Fig. 2a, bottom row, Extended Data Fig. 4c). Consistently, TCRs cloned from T_{Reg} and T_{Ex} clusters, but not those cloned from T_{NExM} clusters, conferred both activation and cytotoxic potential to transduced lymphocytes (Extended Data Fig. 4d).

Direct tumour recognition was not detected for 64 $CD4^+$ TIL TCRs, even though these clonotypes were expanded. We thus explored whether the engagement of such $CD4^+$ clonotypes could be elicited via indirect presentation by APCs, which would process and present tumour antigens in the context of HLA class II even within the TME of HLA class II^{neg} tumours. To test this, we challenged non-tumour-reactive TCRs against autologous APCs (EBV-LCLs) pulsed with lysates of autologous pdMel-CLs (Fig. 2b). Nine TCRs (four from Pt-A and five from Pt-C) recognized tumour antigens when presented on APCs (Fig. 2c, bottom). Such TCR clonotypes exhibited T_{FH}/T_{PE} ($n = 2$) or T_{Reg} ($n = 7$) primary phenotypes, with only T_{Reg} TCRs corresponding to highly clonally expanded TILs (Fig. 2c, top). Together, these results document that $CD4^+$ TILs could be stimulated in the absence of tumour-intrinsic HLA class II expression via indirect presentation of tumour antigens by APCs. This process can apparently elicit either productive (T_{FH}/T_{PE}) or detrimental (T_{Reg}) antitumour responses.

Overall, in all the analysed patients, T_{TE} TCRs were highly enriched in antitumour specificities ($P < 0.0001$, Fig. 2d), whereas T_{NExM} TCRs did not demonstrate substantial tumour recognition. As expected, the frequency of $CD4^+$ TCRs with direct tumour recognition was increased in HLA class II^{pos} melanomas (Fig. 2d, Pt-A vs Pt-C and Pt-D). Presentation of tumour antigens by APCs could result in indirect recruitment of putative immunosuppressive T_{Reg} cells even in HLA class II^{neg} melanoma. HLA class II^{pos} melanomas could directly stimulate not only T_{TE} TCRs or T_{FH}/T_{PE} TCRs, but also many T_{Reg} TCRs, thus conferring these tumour cells with the ability to directly control immune suppression. In line with their high antitumour reactivity, T_{Ex} and T_{Reg} TCR clonotypes were relatively rare among circulating T cells (Extended Data Fig. 5a, b, Supplementary Results) compared with T_{NExM} clones, as determined by tracing TIL TCR β-chains in blood. Moreover, we detected T_{Ex} and T_{Reg} TCRs, respectively, in effector and regulatory fractions sorted from $CD4^+$ circulating T cells (Extended Data Fig. 5c), suggesting that TILs preserve their phenotype even outside the TME.

Specificity of antitumour $CD4^+$ TCRs

To understand how melanomas could engage $CD4^+$ T_{Ex} and T_{Reg} TCR clonotypes within the TME, we investigated the specificity of 131 TCRs from $CD4^+$ TIL (Fig. 3a), including 67 TCRs with direct tumour reactivity and 9 TCRs with indirect recognition of tumour antigens reconstructed from three patients (Pt-A, Pt-C and Pt-D). TCRs were screened against autologous EBV-LCLs pulsed with hundreds of peptides corresponding to: (1) personal neoantigens defined by HLA class I or II prediction pipelines (Methods; Supplementary Table 6) or detected within the HLA class II immunopeptidomes of pdMel-CLs; (2) previously identified melanoma-associated antigens (MAAs), tested as pools of overlapping peptides; or (3) collections of common viral antigens.

We were able to define the antigenic specificity (that is, 'de-orphanize' them) for 30 out of 67 (45%) directly tumour-reactive TCRs (Extended Data Fig. 6a–c), whereas none of the 9 TCRs with indirect tumour antigen reactivity recognized the tested antigens (Fig. 3a). For Pt-A, three T_{TE} TCRs demonstrated specificity for peptides derived from MLANA and TYR pools (Fig. 3b, Extended Data Fig. 6a). Since we observed that these TCRs directly recognized pdMel-CLs from Pt-A—which did not express HLA class II, even upon IFNγ treatment (Fig. 1b)—we tested whether they recognized MAA peptides when presented within the patient's HLA class I restrictions. In co-culture with peptide-pulsed monoallelic HLA class I-expressing targets, TCR-transduced $CD4^+$ effectors recognized their cognate antigens (immunogenic $MLANA_{27–35}$ (ref. [17]) or TYR peptide pools) within HLA class I restrictions (HLA-A*02:01 or HLA-B*44:02; Fig. 3c). TILs expressing these three TCRs were unambiguously confirmed as $CD4^+$ clonotypes on the basis of scRNA-seq and CITE-seq analysis (Extended Data Fig. 7a). Both $CD4^+$ or $CD8^+$ T cells transduced with a $MLANA_{27–35}$-specific TCR isolated from Pt-A $CD4^+$ TILs could bind cognate dextramers (Methods; Extended Data Fig. 7b), demonstrating the low dependency on CD4 or CD8 co-stimulation for these interactions. HLA-A*02:01-restricted $MLANA_{27–35}$–specific $CD4^+$ TILs were directly detectable in samples from Pt-A by multiparametric flow cytometry and were positive for PD-1 and CD39 exhaustion markers and negative for regulatory or memory T-cell markers (CD25, CD127, CD45RA and CCR7)—in concordance with scRNA-seq and CITE-seq data (Extended Data Fig. 7c, d). Of note, HLA class I-restricted $CD4^+$ TILs were highly similar to cytotoxic $CD8^+$ TILs detected within the same TME and specific for the same HLA–peptide complex[13], since they exhibited strong cytotoxic profiles with evidence of degranulation upon stimulation with autologous melanoma (Extended Data Fig. 7d, e). These data demonstrate that $CD4^+$ TILs can harbour HLA class I-restricted TCRs, thereby enabling their tumour-directed cytotoxicity against HLA class II^{neg} tumours.

In Pt-C and Pt-D (both with HLA class II^{pos} melanomas), 25 de-orphanized antitumour TCRs recognized 13 neoantigens with predicted HLA class II restriction (Fig. 3b, Supplementary Table 7); 2 tumour-reactive TCRs from Pt-D cross-recognized viral antigens, whereas no MAA-specific TCR was detected. Whereas MAA-specific TCRs from Pt-A tracked almost exclusively to the T_{TE} compartment, neoantigen-specific TCRs from Pt-C and Pt-D largely harboured T_{Reg} clusters, although expression of T_{Ex} phenotypes was also common (Fig. 3b, d, e). Tumour and viral-crossreactive clonotypes also had T_{Reg} phenotypes, while the few deorphanized non-tumour reactive TCRs ($n = 4$; Fig. 3a) recognized viral targets and were expressed by T_{NExM} TILs (Fig. 3d, e). Despite these phenotypic differences, we found that T_{Ex} or T_{Reg} TCRs had similar wide ranges of avidities (Fig. 3f, Extended Data Fig. 8a, b), which were inversely correlated with tumour antigen abundance, especially for T_{Ex} TCRs ($P = 0.0113$; Extended Data Fig. 8c, d). Together, these data reveal that the HLA class II^{pos} melanoma TME is rich in neoantigen-specific T_{Reg} cells. Further, they suggest an active contribution by neoantigen and HLA class II expression in these tumours to orchestrate interactions with immunosuppressive cells.

HLA class II^{pos} melanomas have high TMB

The clonal expansion of numerous neoantigen-specific T_{Reg} cells in Pt-C and Pt-D appeared to be favoured by extremely high tumour neoantigen burdens (Supplementary Table 1). We thus hypothesized that HLA

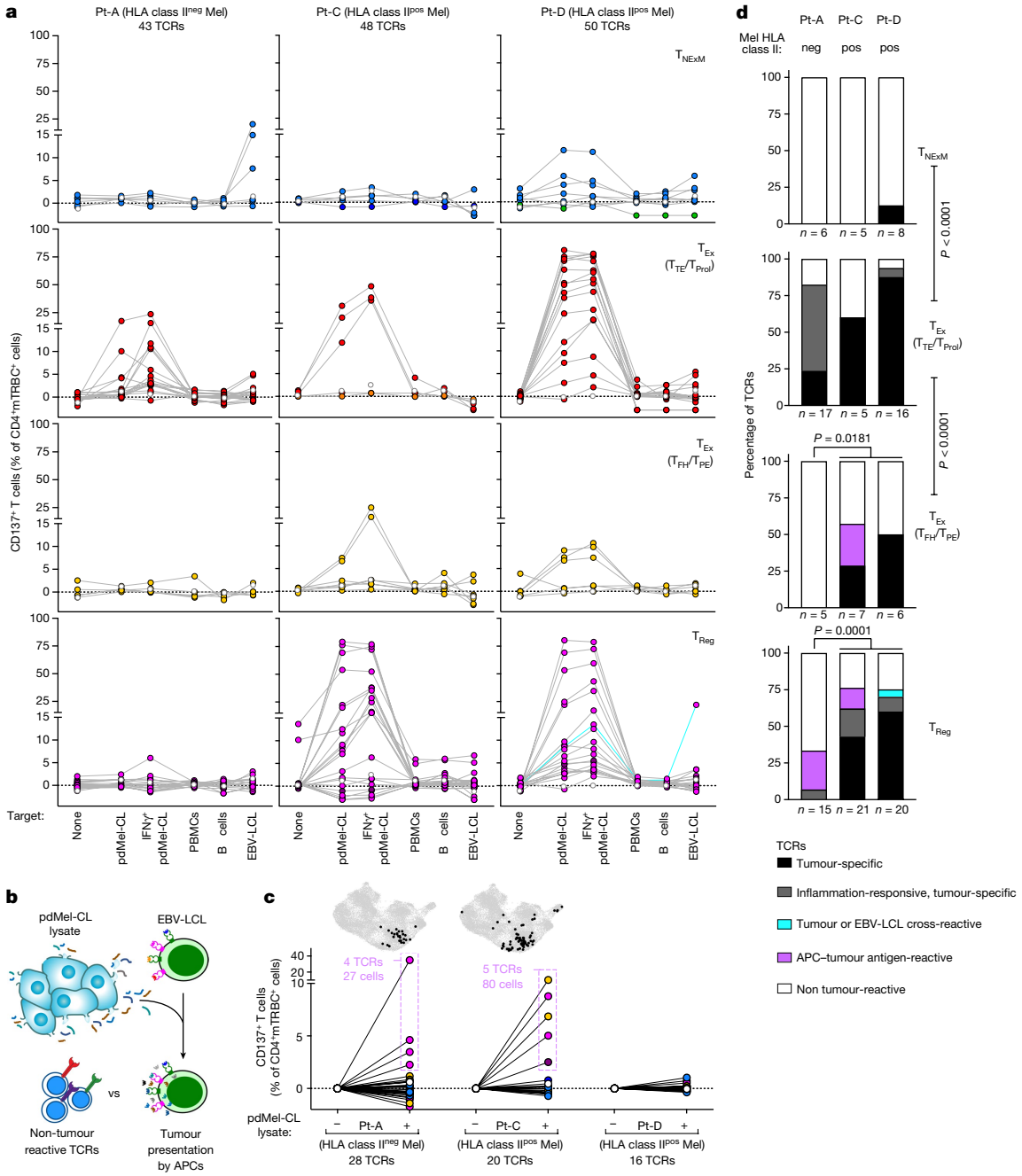

Fig. 2 | Tumour reactivity of TCRs from CD4⁺ TIL. a, Reactivity of the dominant TCRs cloned from CD4⁺ TILs with T_{NExM}, T_{Ex} (divided into T_{TE}/T_{Prol} and T_{FH}/T_{PE}) or T_{Reg} phenotypes in three patients with melanoma. CD137 upregulation was measured on TCR-transduced (mTRBC⁺) CD4⁺ T cells cultured alone (no target) or in the presence of autologous pdMel-CLs (with or without IFNγ pre-treatment) or controls (PBMCs, B cells or EBV-LCLs). Background reactivity of an irrelevant TCR was subtracted (examples in Extended Data Fig. 4b). Dotted lines show behaviour of individual TCRs; dot colours correspond to the phenotypes of TCR clonotypes shown in Fig. 1d; open dots show the signal of untransduced cells and turquoise lines show tumour- and EBV-LCL-cross-reactive TCR. Reactivity of TCRs obtained from Pt-B in Extended Data Fig. 4c. **b**, Workflow for testing indirect antitumour reactivity: autologous APCs (EBV-LCLs) were pulsed with tumour lysates from pdMel-CLs and used to challenge 64 TCRs that did not exhibit direct tumour recognition, as evaluated in **a** (from Pt-A, Pt-C and Pt-D). **c**, TCR reactivity against tumour antigens presented by APCs, measured as upregulation of CD137. PBS-pulsed targets were used as background controls. Dot colours correspond to the phenotypes of TCR clonotypes shown in Fig. 1d. Reactive TCRs were traced (outlined in purple) in CD4⁺ TILs (corresponding to the UMAP in Fig. 1c), to depict abundance and cluster distribution of corresponding TCR clonotypes (top, black dots). **d**, Summary of CD4⁺ TIL TCR reactivity as measured in **a** and **c** for three patients (Pt-A, Pt-C and Pt-D) and classified as detailed in Extended Data Fig. 4a. Percentages of TCR classes are shown for four different CD4⁺ phenotypes. Labels below the *x*-axis show the number of tested TCRs. *P* two-sided Fisher's exact test on total numbers of TCRs with direct antitumour activity (black or grey) tested in each phenotypic compartment, or in HLA class II^{pos} (Pt-C and Pt-D) vs HLA class II^{neg} (Pt-A) melanomas.

class II^{pos} melanoma can tolerate large numbers of mutations, since they would have a rich source of neoantigens from which to expand tumour-specific T_{Reg} cells. We therefore evaluated the relationship between HLA class II expression on melanoma cells (by IHC) and tumour mutation burden (TMB, calculated from bulk sequencing data) in 116 specimens from 4 cohorts (DFCI-Neovax[18], MGH[3], CheckMate

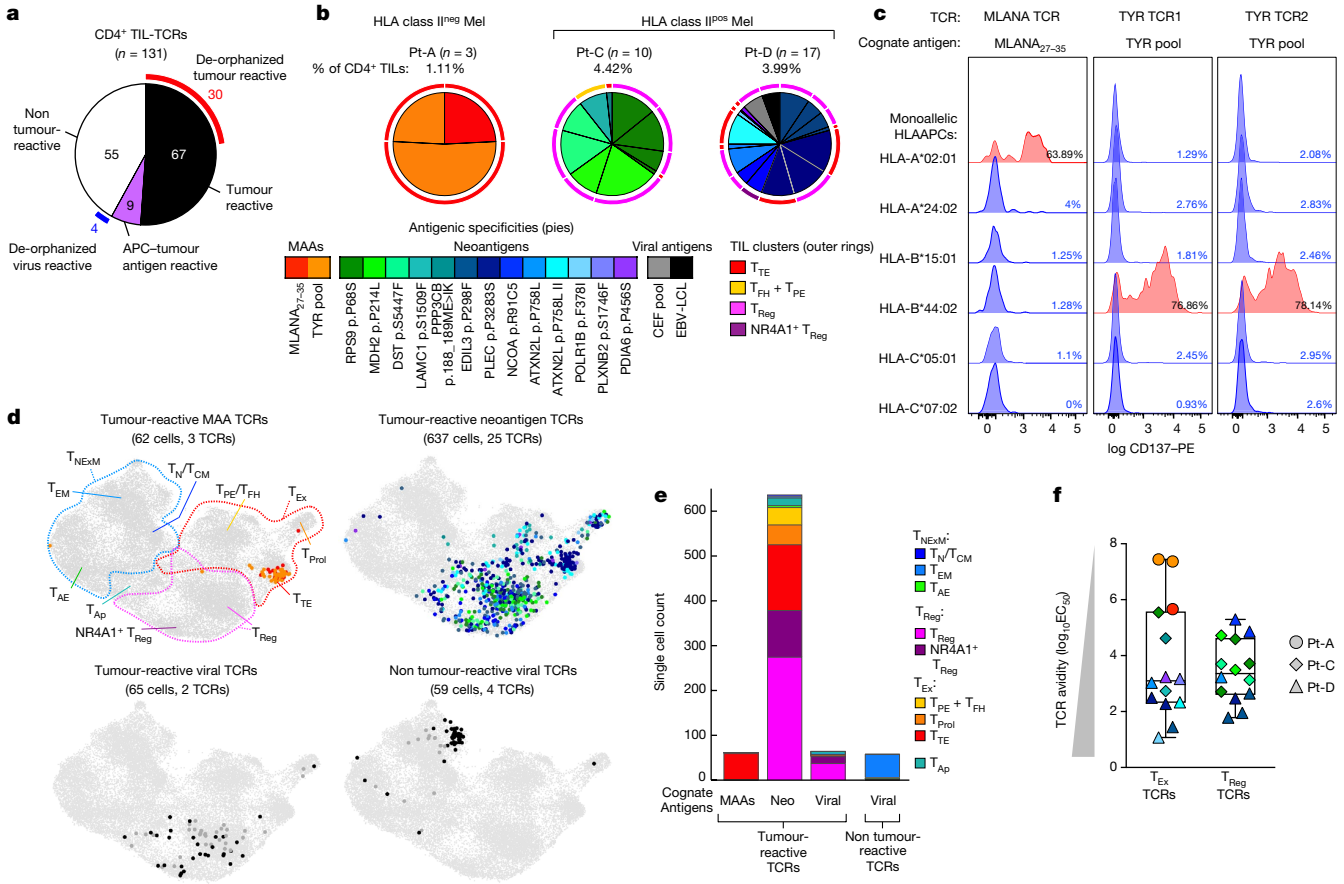

Fig. 3 | Antigen specificity of TCRs from CD4$^+$ TILs. a, Pie chart summarizing the classification of 131 CD4$^+$ TIL TCRs tested for antigen specificity in melanomas from 3 patients (Pt-A, Pt-C and Pt-D). Partial outer ring indicates TCRs with detected antigen specificity (that is, de-orphanized). **b**, Cognate antigens of de-orphanized antitumour TIL TCRs, showing the relative frequency of CD4$^+$ TCR-clonotypes with MAA, neoantigen or viral antigen specificity. Numbers and total frequencies of tested TCR clonotypes among CD4$^+$ TILs are reported above each chart. Pie colours indicate the cognate antigens of the TCR; the outer ring colours show the primary phenotype of the clonotypes. **c**, Deconvolution of HLA class I restriction of 3 de-orphanized tumour-specific CD4$^+$ TCRs from Pt-A. Flow cytometry histograms depict CD137 upregulation measured on CD4$^+$ T cells transduced with TCRs reactive to MLANA$_{27–35}$ peptide ($n = 1$, left) or to TYR peptide pool ($n = 2$, right). TCRs were tested against their cognate antigen, presented by APCs stably transformed with single HLA class I alleles from Pt-A (rows). Red histograms show HLA class I restrictions capable of triggering TCR reactivity upon binding of cognate antigens. **d**, UMAPs of CD4$^+$ TILs bearing antitumour TCRs specific for MAAs, neoantigens or viral antigens, or non tumour-reactive TCRs specific for viral antigens. Dot colours indicate TCR antigenic specificity corresponding to the scheme in **b**. TIL phenotypic clusters are delineated within the first UMAP as reference. **e**, Cell counts of de-orphanized tumour-reactive or non tumour-reactive CD4$^+$ TCR clonotypes specific for different types of cognate antigens (MAAs, neoantigens and viral antigens). Colours show cell states, as inferred by scRNA-seq (Fig. 1c). **f**, Comparison of avidities of de-orphanized antitumour TIL TCRs with T_{Ex} ($n = 14$) or T_{Reg} ($n = 14$) phenotypes. Dot colours show TCR cognate antigens; colour scheme as in **b**. The shapes indicate the patient in whom the TCRs were detected. Whiskers extend from minimum to maximum values; horizontal bars represent the median and boxes encompass 25th–75th percentiles.

064 (ref. [11]) and CheckMate 038 (ref. [19]); Supplementary Table 8). Twenty-eight melanomas (24%) with high HLA class II frequency (score above 10; Methods) had a higher TMB compared with 87 HLA class II^{neg} melanomas ($P < 0.0001$; Fig. 4a). In selected patients, we verified that HLA class II^{pos} melanomas had higher numbers of CD8$^+$ and CD4$^+$ TILs (Extended Data Fig. 9a, b; $P < 0.0001$ and $P = 0.0004$ respectively), probably resulting from recognition of neoantigens derived from their elevated TMB. HLA class II^{pos} melanomas also showed higher levels of HLA class I expression ($P = 0.0005$; Fig. 4b), suggesting that such tumours may use HLA class II upregulation as a mechanism of immune evasion rather than HLA class I downregulation to counteract CD8$^+$ T cell responses[20,21]. The pattern of HLA class I/II expression in melanomas in relation to their TMB (Fig. 4a, Methods) indicated that HLA class I was frequently downregulated in melanomas with low, moderate or high TMB, whereas HLA class II upregulation was enriched among tumours with extremely high TMB ($P < 0.0001$; Fig. 4c). Consistent with previous reports[11,12], overall survival and progression-free survival following immunotherapy treatments were higher for patients with HLA class II^{pos} melanoma than for those with HLA class II^{neg} tumours ($P < 0.0180$ and $P = 0.0136$, respectively; Extended Data Fig. 9c, d, Supplementary Table 8). These outcomes could be ascribed primarily to the high TMB associated with HLA class II^{pos} melanomas (Extended Data Fig. 9e, f), and to the ability to leverage the abundant CD4$^+$ and CD8$^+$ TILs resulting from numerous neoantigens. Our findings implicate HLA class II upregulation as the preferred mechanism in the setting of extreme TMB, since this expression state would endow melanoma cells with the ability to present mutated peptides to CD4$^+$ TILs, thus increasing the chances of engaging immunosuppressive T_{Reg} cells.

Evaluation of TMB and HLA class I/II expression in a comprehensive dataset of 927 human tumour cell lines[22] revealed that only a subset of skin cancer cell lines exhibited levels of HLA class II expression comparable to those in cancers with known HLA class II positivity (that is, haematopoietic malignancies; Extended Data Fig. 10a). Direct comparison of the transcriptional profile of HLA class II^{pos} and HLA class

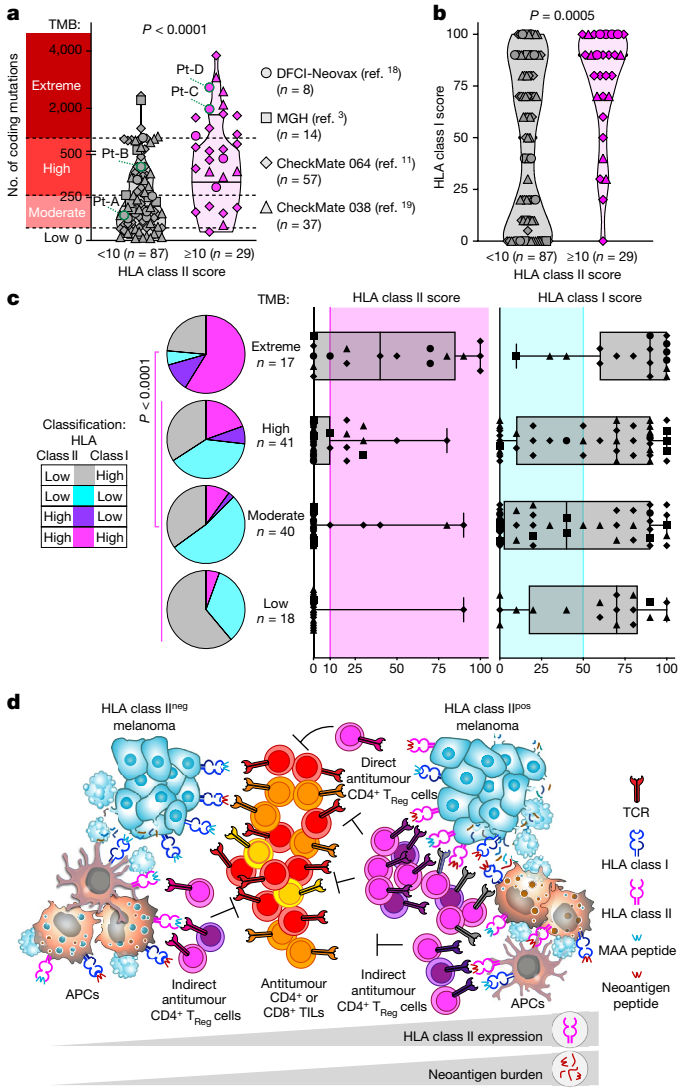

Fig. 4 | Relationship between HLA expression and mutation burden in melanoma. a, **b**, Number of coding mutations (from tumour bulk-sequencing analysis) (**a**) and HLA class I scores (from IHC) (**b**) detected in patients with melanoma from four previous studies[3,11,18,19]; the same shapes represent the studies throughout the figure. Melanomas were classified on the basis of HLA class II expression, scored on tumours by IHC (≥10% or < 10% of SOX10$^+$ melanoma cells). Horizontal lines represent the median (bold) and quartiles; *P* two-sided Mann–Whitney test. Melanomas were divided in four groups on the basis of the TMB (*y*-axis in **a**): low, below 15th percentile; moderate, 15th percentile to median; high, median to 85th percentile; extreme, above 85th percentile. **c**, Tumour HLA class I (top) and HLA class II (bottom) scores determined by IHC of 116 melanoma specimens with different TMB ranges, as established in **a**. Pink area indicates HLA class II upregulation (IHC score ≥ 10%) and turquoise area indicates HLA class I downregulation (IHC score ≤ 50%). Whiskers extend to minimum and maximum values, horizontal bars show the median and boxes encompass 25th–75th percentiles. Pie charts show the proportion of melanomas classified on the basis of HLA class I and class II expression for each TMB category. *P*-value for enrichment of HLA class II^{pos} cases in the extreme TMB group versus non-extreme TMB groups (two-sided Fisher's exact test). **d**, Proposed mechanism of HLA class II-driven immune evasion in melanoma: as well as being able to the indirectly elicit CD4$^+$ responses through APCs, HLA class II^{pos} melanoma with extreme TMB can directly trigger and expand immunosuppressive T_{Reg} cell clones (delineated by different TCR colours) through exposure of HLA class II–neoantigen complexes.

II^{neg} melanoma cell lines revealed that the former were enriched for increased expression of genes related to nervous system differentiation (*SOX2* and *NGFR*) and remodelling of cellular interactions (Extended Data Fig. 10b, c, Supplementary Tables 9, 10). Previous studies have defined an NGFR^{pos} programme within a subset of melanomas with dedifferentiation and increased invasiveness[23,24]. Our data support the notion that HLA class II expression is thus associated with this cancer phenotype and contributes to its evasion from immune control.

Discussion

Although high frequencies of helper or regulatory T cells have been described within the TME of diverse cancers[4–7,25–27], little is known about how tumours engage CD4$^+$ TILs. Here we captured the potential cross-talk between cancer and immune cells by coupling high-resolution single-cell profiling with reconstruction and specificity testing of CD4$^+$ TIL TCRs. Our data draw attention to three general types of potential interactions between tumour-specific CD4$^+$ TILs and melanomas.

First, we confirmed that tumour-specific CD4$^+$ TIL TCRs can be engaged through presentation of tumour antigens by APCs, enabling the induction of CD4$^+$ responses even in absence of tumour HLA class II expression. We ascertained that this indirect pathway of tumour antigen presentation predominantly elicited putative immunosuppressive T_{Reg} cells, as observed recently in mouse models[28]. Thus, in coordination with other immune cells, HLA class II^{neg} tumours can indirectly activate tumour-specific immunosuppressive T_{Reg} cells.

A second class of interactions involves direct engagement of T_{Reg} cells by tumour cells, highlighting the acquisition of immune-evasion capabilities by melanomas that aberrantly express HLA class II. We unambiguously established the direct tumour specificity of more than 70% of T_{Reg} TCRs that were expanded in the TME of two patients with HLA class II^{pos} melanomas. The majority of such TCRs showed specificity for neoantigens with avidities that were similar to those of T_{Ex} TCRs, suggesting that their stimulation could result in activation of putatively immunosuppressive T_{Reg} cells. In Pt-C and Pt-D, this phenomenon was favoured not only by the stable tumour expression of HLA class II, but also by an extremely high TMB. Indeed, HLA class II expression was highly enriched in melanomas with extreme TMBs, as robustly validated in independent specimens. We presume that this association would provide the basis for clonal expansion of functional neoantigen-specific T_{Reg} cells, although definitive demonstration of this effect requires evaluation of additional scRNA-seq and scTCR-seq datasets with the high depth required to detect large numbers of T_{Reg} cells and assess their clonality and functional capabilities. Indeed, the generally low level of expansion of CD4$^+$ clonotypes and the low frequency of HLA class II^{pos} melanomas with extreme TMB (10%) limit validation in existing melanoma datasets[3,29–31]. Nonetheless, the data from Pt-C and Pt-D suggest that by enabling the presentation of numerous neoantigens, expression of HLA class II allows melanomas to engage and control putatively immunosuppressive neoantigen-specific T_{Reg} clones and thereby counterbalance the high immunogenicity that would be otherwise expected from extremely mutated tumours[13,32]. As suggested by the analysis of tumour cell lines, we suspect that aberrant HLA class II expression is particularly enriched in melanomas with a de-differentiated neural crest phenotype[23,24], which may acquire an HLA class II^{pos}SOX2^{pos} state similar to that observed in fetal neural cells[33,34].

Finally, CD4$^+$ T_{Ex} TILs were highly enriched for tumour-specific TCRs, revealing how their interactions with tumour antigens markedly skewed the phenotype of cytotoxic CD4$^+$ T cells towards a highly exhausted state. Such CD4$^+$ TILs could be elicited by HLA class II-restricted neoantigens (as in Pt-C and Pt-D) and by MAA peptides when presented within the context of HLA class I molecules, as verified in Pt-A. These CD4$^+$ TILs harboured CD4- and CD8-independent TCRs and displayed phenotypes and cytotoxicity highly similar to those of antitumour CD8$^+$ TILs. Further studies are required to investigate the incidence of HLA class I-restricted CD4$^+$ TILs, but we speculate that such TILs are more likely to be present when canonical HLA class II-restricted CD4$^+$

responses are poorly favoured (as in the melanoma from Pt-A, which exhibits low HLA class II expression).

This study focused on the in-depth characterization of treatment-naive melanomas. However, HLA class II expression is associated with increased overall survival and progression-free survival after immune checkpoint blockade[11,12]. Indeed, we found that HLA class II^{pos} melanomas were characterized not only by clonal expansion of T_{Reg} cells, but also by high numbers of CD8$^+$ TILs, owing to their association with extreme TMB. Under such conditions, the revival of CD8$^+$ responses may disrupt the equilibrium between effectors and T_{Reg} cells, thus fostering the high immunogenicity expected from HLA class II^{pos} melanomas. Given the importance of direct or indirect engagement of T_{Reg} cells, our study provides a rationale for the development of therapies that might disrupt such interactions to increase the efficacy of immunotherapies such as cancer vaccines or immune checkpoint blockade.

Online content

Any methods, additional references, Nature Research reporting summaries, source data, extended data, supplementary information, acknowledgements, peer review information; details of author contributions and competing interests; and statements of data and code availability are available at https://doi.org/10.1038/s41586-022-04682-5.

1. Sallusto, F. & Lanzavecchia, A. Heterogeneity of CD4$^+$ memory T cells: functional modules for tailored immunity. *Eur. J. Immunol.* **39**, 2076–2082 (2009).
2. Swain, S. L., McKinstry, K. K. & Strutt, T. M. Expanding roles for CD4$^+$ T cells in immunity to viruses. *Nat. Rev. Immunol.* **12**, 136–148 (2012).
3. Sade-Feldman, M. et al. Defining T cell states associated with response to checkpoint immunotherapy in melanoma. *Cell* **175**, 998–1013.e20 (2018).
4. Yost, K. E. et al. Clonal replacement of tumor-specific T cells following PD-1 blockade. *Nat. Med.* **25**, 1251–1259 (2019).
5. Wu, T. D. et al. Peripheral T cell expansion predicts tumour infiltration and clinical response. *Nature* **579**, 274–278 (2020).
6. Oh, D. Y. et al. Intratumoral CD4$^+$ T cells mediate anti-tumor cytotoxicity in human bladder cancer. *Cell* **181**, 1612–1625.e13 (2020).
7. Cachot, A. et al. Tumor-specific cytolytic CD4 T cells mediate immunity against human cancer. *Sci. Adv.* **7**, eabe3348 (2021).
8. Quezada, S. A. et al. Tumor-reactive CD4$^+$ T cells develop cytotoxic activity and eradicate large established melanoma after transfer into lymphopenic hosts. *J. Exp. Med.* **207**, 637–650 (2010).
9. Tanaka, A. & Sakaguchi, S. Regulatory T cells in cancer immunotherapy. *Cell Res.* **27**, 109–118 (2017).
10. Borst, J., Ahrends, T., Bąbała, N., Melief, C. J. M. & Kastenmüller, W. CD4$^+$ T cell help in cancer immunology and immunotherapy. *Nat. Rev. Immunol.* **18**, 635–647 (2018).
11. Rodig, S. J. et al. MHC proteins confer differential sensitivity to CTLA-4 and PD-1 blockade in untreated metastatic melanoma. *Sci. Transl. Med.* **10**, eaar3342 (2018).
12. Johnson, D. B. et al. Melanoma-specific MHC-II expression represents a tumour-autonomous phenotype and predicts response to anti-PD-1/PD-L1 therapy. *Nat. Commun.* **7**, 10582 (2016).
13. Oliveira, G. et al. Phenotype, specificity and avidity of antitumour CD8$^+$ T cells in melanoma. *Nature* **596**, 119–125 (2021).
14. Stoeckius, M. et al. Simultaneous epitope and transcriptome measurement in single cells. *Nat. Methods* **14**, 865–868 (2017).
15. Miller, B. C. et al. Subsets of exhausted CD8$^+$ T cells differentially mediate tumor control and respond to checkpoint blockade. *Nat. Immunol.* **20**, 326–336 (2019).
16. Wolfl, M. et al. Activation-induced expression of CD137 permits detection, isolation, and expansion of the full repertoire of CD8$^+$ T cells responding to antigen without requiring knowledge of epitope specificities. *Blood* **110**, 201–210 (2007).
17. Kawakami, Y. et al. Identification of a human melanoma antigen recognized by tumor-infiltrating lymphocytes associated with in vivo tumor rejection. *Proc. Natl Acad. Sci. USA* **91**, 6458–6462 (1994).
18. Hu, Z. et al. Personal neoantigen vaccines induce persistent memory T cell responses and epitope spreading in patients with melanoma. *Nat. Med.* **27**, 515–525 (2021).
19. Anagnostou, V. et al. Integrative tumor and immune cell multi-omic analyses predict response to immune checkpoint blockade in melanoma. *Cell Rep. Med.* **1**, 100139 (2020).
20. Sade-Feldman, M. et al. Resistance to checkpoint blockade therapy through inactivation of antigen presentation. *Nat. Commun.* **8**, 1136 (2017).
21. Garrido, F. MHC/HLA class I loss in cancer cells. *Adv. Exp. Med. Biol.* **1151**, 15–78 (2019).
22. Ghandi, M. et al. Next-generation characterization of the Cancer Cell Line Encyclopedia. *Nature* **569**, 503–508 (2019).
23. Landsberg, J. et al. Melanomas resist T-cell therapy through inflammation-induced reversible dedifferentiation. *Nature* **490**, 412–416 (2012).
24. Boshuizen, J. et al. Reversal of pre-existing NGFR-driven tumor and immune therapy resistance. *Nat. Commun.* **11**, 3946 (2020).
25. Guo, X. et al. Global characterization of T cells in non-small-cell lung cancer by single-cell sequencing. *Nat. Med.* **24**, 978–985 (2018).
26. Ahmadzadeh, M. et al. FOXP3 expression accurately defines the population of intratumoral regulatory T cells that selectively accumulate in metastatic melanoma lesions. *Blood* **112**, 4953–4960 (2008).
27. De Simone, M. et al. Transcriptional landscape of human tissue lymphocytes unveils uniqueness of tumor-infiltrating T regulatory cells. *Immunity* **45**, 1135–1147 (2016).
28. Marangoni, F. et al. Expansion of tumor-associated T_{reg} cells upon disruption of a CTLA-4-dependent feedback loop. *Cell* **184**, 3998–4015.e19 (2021).
29. Li, H. et al. Dysfunctional CD8 T cells form a proliferative, dynamically regulated compartment within human melanoma. *Cell* **176**, 775–789.e18 (2019).
30. Tirosh, I. et al. Dissecting the multicellular ecosystem of metastatic melanoma by single-cell RNA-seq. *Science* **352**, 189–196 (2016).
31. Jerby-Arnon, L. et al. A cancer cell program promotes T cell exclusion and resistance to checkpoint blockade. *Cell* **175**, 984–997.e24 (2018).
32. Jhunjhunwala, S., Hammer, C. & Delamarre, L. Antigen presentation in cancer: insights into tumour immunogenicity and immune evasion. *Nat. Rev. Cancer* **21**, 298–312 (2021).
33. Vagaska, B. et al. MHC-class-II are expressed in a subpopulation of human neural stem cells in vitro in an IFNγ-independent fashion and during development. *Sci Rep.* **6**, 24251 (2016).
34. Diener, J. & Sommer, L. Reemergence of neural crest stem cell-like states in melanoma during disease progression and treatment. *Stem Cells Transl. Med.* **10**, 522–533 (2021).

Methods

Study subjects and patient samples

Single-cell sequencing and TCR-screening analyses were conducted on a discovery cohort of 4 patients (Pt-A, Pt-B, Pt-C and Pt-D) with high-risk melanoma enrolled between May 2014 and July 2016 to a single-centre, phase I clinical trial approved by the Dana-Farber/Harvard Cancer Center Institutional Review Board (IRB) (NCT01970358, DFCI-Neovax). This study was conducted in accordance with the Declaration of Helsinki. The details about eligibility criteria have been described previously[13,18,35], and all subjects received neoantigen-targeting peptide vaccines, as previously reported (Supplementary Table 1). Tumour samples were obtained immediately following surgery and processed as previously described[13,18,35] for single-cell analyses. Heparinized blood samples were obtained from the same study subjects on IRB-approved protocols at Dana-Farber Cancer Institute (DFCI).

For collection of the melanoma specimens listed in Supplementary Table 3, tumour tissues were procured under IRB-approved protocols (06-375) at Brigham and Women's Hospital.

The analysis was extended to all the patients treated within the DFCI-Neovax trial[18], and to three additional independent cohorts of melanoma patients treated with immune checkpoint blockade therapy, as previously reported[3,11,19]. These included patients from CheckMate 064 (NCT01783938) and CheckMate 038 (NCT01621490) clinical trials. All the patients from whom anonymized specimens were obtained and analysed (Supplementary Tables 3, 8) provided written informed consent for the collection of tissue samples for research and genomic profiling.

Sequencing of melanoma cell lines and parental tumours

Whole-exome sequencing (WES) and RNA sequencing (RNA-seq) of patients or cell lines from the discovery cohort were analysed as previously reported[13,18,35] and as described in the Supplementary Information. For patients from validation cohorts, mutations sequenced by WES or RNA-seq were annotated from corresponding published studies[3,11,18,19]. To determine the TMB of melanomas, mutations in gene-coding regions and resulting in modifications of the wild-type amino acid sequence (coding mutations) were counted and the total number of coding mutations were reported per tumour sample. Melanomas were divided into 4 subgroups on the basis of TMB (Fig. 4a): specimens above the 85th percentile were included within the extreme TMB subgroup; the 15th percentile was used to define the cases with low TMB, based on symmetry. The median marked the difference between melanomas with moderate (15th percentile to median) versus high (median to 85th percentile) TMB.

Processing of single-cell data

Processing of scTCR-seq data. TCR-seq data were processed using Cell Ranger software (version 3.1.0). On the basis of TCRα–TCRβ chain identity, TCRs were grouped in patient-specific TCR clonotype families allowing for a single amino acid substitution within the TCRα–TCRβ CDR3s. Cells with a single TCR chain were included; the resulting TCR clonotype families were incorporated into downstream analysis. This procedure was reiterated on all samples sequenced from the same patient and results were manually reviewed. Owing to the low number of TCR clonotypes specific for the Pt-C relapse specimen ($n = 7$), Pt-C and Pt-C relapse TILs were analysed together (referred to as Pt-C within the text).

Processing and analysis of scRNA-seq and CITE-seq data. scRNA-seq data were processed with Cell Ranger software (version 3.1.0). scRNA-seq count matrices and CITE-seq antibody expression matrices were read into Seurat[36] (version 3.2.0). For each batch of samples comprising all tumour or PBMC single-cell data acquired for a single patient, a Seurat object was generated. Cells were filtered to retain those with ≤20% mitochondrial RNA content and with a number of unique molecular identifiers (UMIs) comprised between 250 and 10,000. For TIL analysis, scTCR-seq data were integrated and cells with ≥3 TCRα chains, ≥3 TCRβ chains or 2 TCRα and 2 TCRβ chains were removed. scRNA-seq and data CITE-seq were normalized using Seurat NormalizeData function and the centre log-ratio (CLR) function respectively. CITE-seq signals were then expressed as relative to isotype controls signals of each single cell, dividing each antibody signal by the average signal from three CITE-seq isotype control antibodies. For cells with an average isotype signal less than 1, all the corresponding CITE-seq signals were increased of a value equal to 1 − mean isotype signal.

Each patient dataset was scaled and processed under principal component analysis using the ScaleData, FindVariableFeatures and RunPCA functions in Seurat. Serial custom filters were used to identify $CD4^+$ T lymphocytes: first, UMAP areas with predominance of cells belonging to FACS-sorted $CD45^+CD3^+$ populations and with high density of *CD3E* transcripts were selected. Second, possible contaminants belonging to B and myeloid lineages were removed by excluding cells with high expression of *CD19* and *ITGAM* transcripts or positivity for CD19 or CD11b CITE-seq antibodies. Remaining events were grouped in $CD8^+$ or $CD4^+$ cells using the corresponding CITE-seq antibodies, and $CD4^+CD8^-$ TILs were selected[13]. Importantly, these steps were designed to maximize the ability to correctly detect $CD4^+$ T cells by relying on the actual surface protein expression of CD4, thus avoiding cell loss due to possible false negatives at the RNA level. Cells classified as $CD4^+CD8^-$ from tumour specimens of the four patients were combined using the RunHarmony function in Seurat with default parameters[37]. Data were normalized and scaled and principal components computed as previously described. UMAP coordinates, neighbours and clusters were calculated with the reduction parameter set to 'harmony' to identify clusters of cells. Cluster stability over objects with different resolutions was evaluated to select the appropriate level of resolution (0.6). Clusters composed of less than 100 cells were not characterized. Markers specific for each cluster were found using Seurat's FindAllMarkers function with min.pct set to 0.25 and logfc.threshold set to log(2) (Supplementary Table 5). Cluster classification was performed using RNA and surface protein expression of a panel of T cell-related genes and by cross-labelling with reference gene signatures from external single-cell datasets of human TILs[4–6] (see Supplementary Information).

Phenotypic distribution of TCR clonotypes composed by >1 cell (defined as TCR clonotype families) was examined using the $CD4^+$ clusters identified through Seurat clustering. To associate a cell state with each TCR clonotype family, a 'primary cluster' or 'primary phenotype' was assigned by selecting the cluster with the largest representation of cells in the clone. No primary cluster was assigned in case of a tie.

For analysis of tumour-enriched fractions ($CD45^-$ single cells), we first selected in each patient the events from samples containing tumour cells ($CD45^-CD3^-$ fractions or unsorted tumour specimens) and then removed cells and clusters previously identified as T cells or other immune types. The remaining cells from all tumour biopsies were then combined and classified based on expression of cell markers, as described[38] (Extended Data Fig. 1b). Clusters constituted by cells from individual patients were classified as tumours by analysing the expression of melanoma-associated markers (*MLANA*, *TYR*, *PMEL* and *PRAME*), as depicted in Extended Data Fig. 1c.

Comparisons with other datasets

Previously published scRNA-seq, scTCR-seq and bulk TCR-seq data reanalysed here are available from gene expression omnibus under accession codes GSE123814 (ref. [4]), GSE139555 (ref. [5]), GSE149652 (ref. [6]) or from the portal[22] www.broadinstitute.org/ccle.

We used the SingleR package to compute reference signatures from the Yost et al., Wu et al. and Oh et al. datasets[4–6]. Count matrices were downloaded from the Gene Expression Omnibus (GSE123814, GSE139555 and GSE149652, respectively). The scater package was used

to normalize expression values for SingleR, and 10% trimmed means for each gene across cells in clusters classified as CD4-related (Oh et al. datasets[6]) or across cells without *CD8A/CD8B* transcript expression (Yost et al. and Wu et al. datasets[4,5]) were calculated. These data were used to train SingleR for classification of the $CD4^+$ TIL internal dataset upon normalization with the same scater function. Counts of cells based on the internal cluster assignment and external assignments performed with SingleR were computed and normalized as described[5], resulting in the matrices reported in Extended Data Fig. 2d.

TCR reconstruction and expression in T cells for reactivity screening

In vitro TCR reconstruction and antigen specificity screening was performed for TCRs from $CD4^+$ TILs of the discovery cohort, selected to be highly expanded within the intratumoural microenvironment or having a primary phenotype representative of all the clusters classified as T_{Ex}, T_{NExM} or T_{Reg}. Selection criteria also included: (1) the availability of reliable sequences for both TCRα and TCRβ chains; (2) the absence of the tested TCRα–TCRβ pairs among $CD8^+$ TILs[13]; and (3) the absence of multiple TCRα or TCRβ chains.

The full-length TCRα and TCRβ chains, separated by a Furin SGSG P2A linker, were synthesized in the TCRβ–TCRα orientation (Integrated DNA Technologies) and cloned into a lentiviral vector (LV) under the control of the pEF1α promoter using Gibson assembly[13] (New England Biolabs). Full-length TCRα V-J regions and TCRβ V-D-J regions were fused to optimized mouse *TRA* and *TRB* constant regions respectively, to allow preferential pairing of the introduced TCR chains, enhanced surface expression and functionality[39–41]. Up to 96 TCRs were cloned in parallel in 96-well plates; the assembled plasmids were transfected in 5-alpha competent *Escherichia coli* bacteria (New England Biolabs). After expansion of bacteria in LB broth (ThermoFisher Scientific) supplemented with ampicillin (Sigma), plasmids were purified using the 96 Miniprep Kit (Qiagen), resuspended in water and sequence-verified through standard sequencing (Eton).

T cells were isolated from PBMCs obtained by healthy individuals using the Pan-T cell selection kit (Miltenyi Biotech) and then activated with antiCD3/CD28 dynabeads (Gibco) in the presence of 5 ng ml^{-1} IL-7 and IL-15 (Peprotech) in 96-well plates. After 1 day, activated cells were transduced with a lentivirus encoding the reconstructed TCRβ and TCRα chains. In brief, lentivirus particles were produced by transient transfection of the lentiviral packaging Lenti-X 293T cells (Takara) with the TCR-encoding and packaging plasmids (VSVg and PSPAX2 (ref. [42])) using Transit LT-1 (Mirus). Parallel production of different lentiviruses encoding diverse TCRs was achieved by seeding packaging cells in 96-well plate format. Lentivirus supernatants were collected each day for 3 consecutive days (days 1, 2 and 3 after transfection) and used on activated T cells on days 1, 2 and 3 after activation. To increase the transduction efficiency, spinoculation (2,000 rpm, 2 h, 37 °C) in the presence of 8 μg ml^{-1} polybrene (ThermoFisher Scientific) was performed at day 2. Beads were removed six days after activation using Dynal magnets and supernatant was replaced with complete medium supplemented with cytokines. Transduction efficiency was assessed quantifying by flow cytometry the percentage of T cells expressing the murine TCRβ with the anti-mouse TCRβ antibody (PE, clone H57-597, 1:50, eBioscience). Cells were also labelled with anti-human CD3 (PE–Cy7, clone UCHT1, 1:50, Biolegend), CD4 (Pacific Blue, clone OKT4, 1:30, Biolegend) and CD8a (BV785, clone RPA-T8, 1:100, Biolegend) antibodies to assess purity of T cell subpopulations: all $CD8^-$ cells were verified to be $CD3^+CD4^+$ and thus $CD3^+CD8^-$ cells were considered as $CD4^+$. T cells were used 14 days after transduction for TCR reactivity tests, as detailed below.

CD137 upregulation assay

TCR signal transduction resulting from antigen recognition was assessed by measuring the upregulation of CD137 surface expression on effector T cells upon co-culture with target cells. To enable simultaneous evaluation of up to 64 distinct TCRs, T cell lines expressing distinct reconstructed TCRs were pooled after labelling with a combination of cytoplasmic dyes, as previously described[13]. In brief, TCR-transduced T cell lines were washed, resuspended in PBS at 1×10^6 cells per ml and labelled with a combination of 3 dyes (Cell Trace CFSE, Far Red or Violet Proliferation Kits, Life Technologies). Up to 4 dilutions per dye were created and then mixed, resulting in up to 64 colour combinations. After incubation at 37 °C for 20 min, T cells were washed twice, resuspended in complete medium and divided in pools. Internal controls were included in each pool; controls consisted in mock-transduced lymphocytes and in T cells transduced with an irrelevant TCR. Effector pools were plated in 96-well plates (0.25×10^6 cells per well) with the following targets: (1) pdMel-CLs (0.25×10^5 cells per well), either untreated or pre-treated with IFNγ (2,000 U ml^{-1}, Peprotech); (2) patient PBMCs (0.25×10^6 cells per well); (3) patient B cells (0.25×10^6 cells per well), purified from PBMCs using anti-human CD19 microbeads (Miltenyi Biotec); (4) patient EBV-LCLs (0.25×10^6 cells per well) alone or pulsed with peptides; (5) medium, as negative control; (6) phytohemagglutinin (2 μg ml^{-1}, Sigma-Aldrich) or PMA (50 ng ml^{-1}, Sigma-Aldrich) and ionomycin (10 μg ml^{-1}, Sigma-Aldrich) as positive controls.

Peptide pulsing of target cells was performed by incubating EBV-LCLs in FBS-free medium at a density of 5×10^6 cells per ml for 2 h in the presence of individual peptides (10^7 pg ml^{-1}, Genscript) or peptide pools (each at 10^7 pg ml^{-1}, JPT Technologies) diluted in ultrapure DMSO (Sigma-Aldrich). Tested peptides comprised pools of: (1) HLA class I-restricted peptides (>70% purity) predicted from patient neoantigens, as previously reported[35] (Supplementary Table 6); (2) HLA class II restricted peptides (>70% purity) predicted from patient neoantigens using NetMHCIIpan[43] (Supplementary Table 6); (3) overlapping 15mer peptides (>70% purity) spanning the entire length of 12 MAA genes (MAGE-A1, MAGE-A3, MAGE-A4, MAGE-A9, MAGE-C, MAGE-D, MLANA, PMEL, TYR, DCT, PRAME, NYESO-1); (4) class I and II peptides (>70% purity) encoding immunogenic viral antigens (CEF pools, JPT Technologies); (5) neoantigen peptides (>70% purity or crude) detected by mass spectrometry within HLA class II binding immunopeptidomes of pdMel-CLs (Supplementary Table 6). In selected experiments, pulsing of EBV-LCLs was performed using pdMel-CL lysates, obtained by repeated cycles of freezing (in dry ice) and thawing (at 37 °C) of melanoma cells.

Following overnight co-incubation of effector and target cells, TCR reactivity was assessed by flow cytometric detection of CD137 upregulation on $CD8^-$ (considered as $CD4^+$)-transduced T cells, using the following antibodies: anti-human CD8a (BV785, clone RPA-T8, 1:100, Biolegend), anti-mouse TRBC (PE-Cy7, clone H57-597, 1:50, eBioscience) and anti-human CD137 (PE, clone 4B4-1, 1:50, Biolegend). Data were acquired on a high throughput sampler (HTS)-equipped Fortessa cytometer (BD Biosciences) and analysed using Flowjo v10.3 software (BD Biosciences). CD137 upregulation was analysed on each effector subpopulation, upon gating of $CD4^+$ ($CD8^-$) mTRBC+ cells, and with downstream gating strategy as described[13]. For each tested condition, background signal measured on $CD4^+$ T cell transduced with an irrelevant TCR was subtracted. Based on CD137 upregulation upon challenge with the different targets, each TCR was classified as described in Extended Data Fig. 4a. A TCR was considered tumour-reactive if the level of background-subtracted CD137 upon coculture with melanoma cells was at least 3% with 2 × s.d. higher than that of the unstimulated control (mean value from 3 replicates per condition). Activation-dependent TCR downregulation was manually evaluated to further corroborate ongoing TCR signal transduction.

In peptide deconvolution analyses, peptide recognition was calculated by subtracting the background detected with DMSO-pulsed EBV-LCLs from the CD137 upregulation level measured from the peptide-pulsed EBV-LCLs. Those TCR reactivities that were detected against target pulsed with crude peptides were subsequentially validated using >90% pure peptides. When TCRs specific for individual

peptides were identified, reactivity was validated and titrated using EBV-LCL cells pulsed with increasing doses of pure peptides (from 10^0 to 10^8 pg ml^{-1}). For neoantigen-specific TCRs, titration was performed for both mutated and wild-type antigens. To define the recognition affinity for each TCR-peptide pair, results of titration curves were normalized, and EC_{50} values were calculated using GraphPad Prism 9 software.

Finally, in selected experiments, deconvolution of HLA class I restriction of selected de-orphanized CD4$^+$ TCRs was performed by testing TCR against the corresponding cognate antigen, presented by monoallelic APCs stably transformed with single patient's HLAs, as available from previous published studies[44,45].

Immunohistochemistry staining and scoring

The procedure of HLA class I/II IHC of formalin fixed-paraffin embedded tumour specimens was previously described[11]. In brief, dual IHC for HLA class I (HLA-A, HLA-B and HLA-C, clone EMR8-5, 1:6,000; Abcam) or HLA class II (HLA-DR, HLA-DP and HLA-DQ, clone CR3/43 or CR3/45, 1:750; Dako) with the melanoma marker SOX10 (clone EP268, 1:1,500; Cell Marque) was performed by Brigham and Women's Hospital Pathology Core (Boston, MA, USA) using an automated staining system[46] (Bond-III, Leica Biosystems).

HLA class I/II staining was scored as the percentage of malignant cells (in 10% increments: 0 to 100%) with positive membrane staining within the entire tissue section, as determined by a pathologist, as previously reported[46]. Malignant cells were defined by nuclear staining for the melanoma marker SOX10 and were only scored if they were nucleated and viable. Necrotic or fibrotic tissue was excluded from the analysis. Any HLA class I or II expression in nonmalignant (SOX10-negative) inflammatory cells served as an internal positive staining control. HLA class II was considered upregulated when the IHC score was ≥10%, while HLA class I was considered downregulated when the IHC score was ≤50%.

IHC staining and quantification of CD8$^+$ and CD4$^+$ of tumour specimens collected from selected patients from CheckMate 064 cohort has been described previously[11]. For selected patients from DFCI-Neovax and MGH cohorts, CD8$^+$ and CD4$^+$ TILs were quantified through immunofluorescence (see Supplementary Information).

Statistical analyses

The following statistical tests were used in this study, as indicated throughout the text: (1) Spearman's correlation coefficients and associated two-sided *P* values were computed using R to test the null hypothesis that the correlation coefficient is zero (Fig. 1e); (2) two-tailed Fisher's exact test were performed using GraphPad Prism 9 to calculate significance of deviation of a distribution from the null hypothesis of no differential distribution (Figs. 2d, 4c); (3) Mann–Whitney tests were performed using the GraphPad Prism 9 software to compare ranks of TMB and HLA expression in melanoma with different HLA class II scores (Fig. 4); (4) ratio-paired parametric *t*-tests were performed using the GraphPad Prism 9 software, to obtain the two-sided *P* value of the null hypothesis that the paired values of two groups have ratio equal to 1 (Extended Data Fig. 7d); (5) linear regressions were performed on log-transformed values of different parameters using GraphPad Prism 9 software, which provided R^2 values and two-sided *P* value of the null hypothesis that the regression coefficient is zero (Extended Data Fig. 8d); (6) log-rank Mantel–Cox test was calculated with GraphPad Prism 9 software, to compare estimates of the hazard function between 2 or 4 groups (Extended Data Fig. 9c–f); (7) normalized Shannon index (Extended Data Fig. 3b) was calculated on patient-specific TCRs or on all available TCR clonotypes as follows:

$$\mathrm{normSI} = \frac{-\sum_{i=1}^{k} fi \log(fi)}{\log(k)}$$

where k is the number of TCR clonotypes, n is the total count of cells and f is frequency.

No statistical methods were used to predetermine sample size.

Reporting summary

Further information on research design is available in the Nature Research Reporting Summary linked to this paper.

Data availability

The scRNA-seq, TCR-seq and CITE-seq sequencing results are available through the dbGaP portal (study ID 26121, accession number phs001451.v3.p1). All other data and codes are presented in the main text or in the supplementary materials and are available from the corresponding authors upon reasonable request.

Code availability

Code used for data analysis included the Broad Institute Picard Pipeline (WES and RNA-seq), GATK4 v4.0, Mutect2 v2.7.0 (single nucleotide variants (SNV) and indel identification), NetMHCpan 4.0 and NetMHCIIpan 4.0 (neoantigen binding prediction), ContEst v1 (contamination estimation), ABSOLUTE v1.1 (purity/ploidy estimation), STAR v2.6.1c (sequencing alignment), RSEM v1.3.1 (gene expression quantification), Seurat v3.2.0 (single-cell sequencing analysis), Harmony v1.0 (single-cell data normalization), SingleR v3.22 (scater package), Scanpy v1.5.1, Python v3.7.4 (for comparison with other single-cell datasets), EdgeR (to compare bulk RNA-seq expression), EnrichR (to analyse enrichment of gene ontologies) that are each publicly available. Custom computer code used to generate the analyses is available at https://github.com/kstromhaug/oliveira-stromhaug-cd4-code.

35. Ott, P. A. et al. An immunogenic personal neoantigen vaccine for patients with melanoma. *Nature* **547**, 217–221 (2017).
36. Stuart, T. et al. Comprehensive integration of single-cell data. *Cell* **177**, 1888–1902.e21 (2019).
37. Korsunsky, I. et al. Fast, sensitive and accurate integration of single-cell data with Harmony. *Nat. Methods* **16**, 1289–1296 (2019).
38. Solé-Boldo, L. et al. Single-cell transcriptomes of the human skin reveal age-related loss of fibroblast priming. *Commun. Biol.* **3**, 188 (2020).
39. Cohen, C. J., Zhao, Y., Zheng, Z., Rosenberg, S. A. & Morgan, R. A. Enhanced antitumor activity of murine-human hybrid T-cell receptor (TCR) in human lymphocytes is associated with improved pairing and TCR/CD3 stability. *Cancer Res.* **66**, 8878–8886 (2006).
40. Haga-Friedman, A., Horovitz-Fried, M. & Cohen, C. J. Incorporation of transmembrane hydrophobic mutations in the TCR enhance its surface expression and T cell functional avidity. *J. Immunol.* **188**, 5538–5546 (2012).
41. Bialer, G., Horovitz-Fried, M., Ya'acobi, S., Morgan, R. A. & Cohen, C. J. Selected murine residues endow human TCR with enhanced tumor recognition. *J. Immunol.* **184**, 6232–6241 (2010).
42. Hu, Z. et al. A cloning and expression system to probe T-cell receptor specificity and assess functional avidity to neoantigens. *Blood* **132**, 1911–1921 (2018).
43. Reynisson, B. et al. Improved prediction of MHC II antigen presentation through integration and motif deconvolution of mass spectrometry MHC eluted ligand data. *J. Proteome Res.* **19**, 2304–2315 (2020).
44. Sarkizova, S. et al. A large peptidome dataset improves HLA class I epitope prediction across most of the human population. *Nat. Biotechnol.* **38**, 199–209 (2020).
45. Abelin, J. G. et al. Mass spectrometry profiling of HLA-associated peptidomes in mono-allelic cells enables more accurate epitope prediction. *Immunity* **46**, 315–326 (2017).
46. Roemer, M. G. M. et al. Classical Hodgkin lymphoma with reduced β2M/MHC class I expression is associated with inferior outcome independent of 9p24.1 status. *Cancer Immunol. Res.* **4**, 910–916 (2016).
47. Restivo, G. et al. low neurotrophin receptor CD271 regulates phenotype switching in melanoma. *Nat. Commun.* **8**, 1988 (2017).
48. Kuleshov, M. V. et al. Enrichr: a comprehensive gene set enrichment analysis web server 2016 update. *Nucleic Acids Res.* **44**, W90–W97 (2016).
49. Paul, P. et al. A Genome-wide multidimensional RNAi screen reveals pathways controlling MHC class II antigen presentation. *Cell* **145**, 268–283 (2011).

Acknowledgements We thank O. Olive, K. Shetty, S. Pollock, C. Patterson, J. L. Weirather and A. Giobbie-Hurder for expert assistance; F. S. Hodi (DFCI Department of Medical Oncology) for help in collection and management of samples and data; and D. Y. Oh, L. Fong, D. M. Pardoll, K. N. Smith, A. Dykema and all members of the Wu laboratory for productive discussions. The authors thank Bristol-Myers Squibb for supporting the work through its International Immuno-Oncology Network. This research was made possible by a generous gift from the Blavatnik Family Foundation, and was supported by grants from the National Institutes of Health (NCI-1R01CA155010; NCI-U24CA224331 (to C.J.W.); NIH/NCI R21 CA216772-01A1 and

NCI-SPORE-2P50CA101942-11A1 (to D.B.K); NCI-1R01CA229261 (to P.A.O.); NIH/NCI P01CA229092, NIH/NIAID U19 AI082630 (to K.J.L.); NCI R50CA251956 (to S.L.), R01 CA208756 (to N.H.); NCI K12CA090354 (J.B.I.)), a Conquer Cancer Foundation/Sontag Foundation grant (to J.B.I.), and a Team Science Award from the Melanoma Research Alliance (to C.J.W. and P.A.O.). G.O. was supported by the American Italian Cancer Foundation fellowship. D.A.B. is supported by the DF/HCC Kidney Cancer SPORE (NCI P50CA101942-15) and the DOD CDMRP Academy of Kidney Cancer Investigators (KC190128). This work was further supported by The G. Harold and Leila Y. Mathers Foundation, and the Bridge Project, a partnership between the Koch Institute for Integrative Cancer Research at MIT and the Dana-Farber/Harvard Cancer Center.

Author contributions G.O. conceived the project. G.O. and C.J.W. directed the overall study. G.O. designed and performed experimental and data analysis. G.O. and K.S. analysed single-cell and bulk sequencing data. G.O. performed TCR reconstruction and screening experiments. W.Z. contributed to plasmid production. G.O., K.S. and D.N. designed and performed statistical analyses. S.L. and K.J.L. performed and analysed scRNA-seq and bulk and scTCR-seq. S.K., S.R., V.C., D.B.K. and S.A.C. generated and analysed mass spectrometry results. S.S.F. performed TMB analysis of the MGH cohort. K.K., D.T.F., C.H.Y., G.M.B., M.W.-R., M.S.-F. and P.A.O. provided patient samples and clinical information and discussed clinical data. J.O.W. generated IHC and immunofluorescence imaging data. S.J.R. and J.B.I. scored IHC stainings. N.C., D.A.B., E.F.F. and N.H. contributed to data discussion and interpretation. G.O. and C.J.W. wrote the manuscript; all authors discussed the results and read the manuscript.

Competing interests E.F.F. is an equity holder and consultant for BioNTech, and equity holder and scientific advisory board member of BioEntre. N.H. and C.J.W. are equity holders of BioNTech. N.H. is an advisor and equity holder for Related Sciences, and receives research funding from Bristol-Myers Squibb. P.A.O. has received research funding from and has advised Neon Therapeutics, Bristol-Myers Squibb, Merck, CytomX, Pfizer, Novartis, Celldex, Amgen, Array, AstraZeneca/MedImmune, Armo BioSciences, Xencor, Oncorus, Phio Pharmaceuticals, Evaxion and Roche/Genentech. C.J.W. is subject to a conflict-of-interest management plan for the reported studies because of her former competing financial interests in Neon Therapeutics, which was acquired by BioNTech. Under this plan, C.J.W. may not access identifiable data for human subjects or otherwise participate directly in the Institutional Review Board-approved protocol reported herein. C.J.W.'s contributions to the overall strategy and data analyses occurred on a de-identified basis. Patent applications have been filed on aspects of the described work entitled as follows: 'Compositions and methods for personalized neoplasia vaccines' (N.H., E.F.F. and C.J.W.), 'Methods for identifying tumour specific neo-antigens' (N.H. and C.J.W.), 'Formulations for neoplasia vaccines' (E.F.F.) and 'Combination therapy for neoantigen vaccine' (N.H., C.J.W. and E.F.F.). The Dana-Farber Cancer Institute has a proprietary and financial interest in the personalized neoantigen vaccine. S.J.R. has research funding from Bristol-Myers-Squibb and KITE/Gilead. S.J.R. is a member of the scientific advisory board of Immunitas Therapeutics. D.A.B. reports personal fees from LM Education and Exchange, Adnovate Strategies, MDedge, Cancer Network, Cancer Expert Now, OncLive, Catenion, AVEO, and grants and personal fees from Exelixis, outside the submitted work. M.S.-F. receives research funding from Bristol-Myers Squibb. M.W.-R. was an employee of Bristol-Myers Squibb and holds equity in Bristol-Myers Squibb. D.B.K. has previously advised Neon Therapeutics and has received consulting fees from Neon Therapeutics. D.B.K. owns equity in Affimed N.V., Armata Pharmaceuticals, Breakbio, BioMarin Pharmaceutical, Bristol-Myers Squibb, Celldex Therapeutics, Editas Medicine, Exelixis, Gilead Sciences, Immunitybio, ImmunoGen, IMV, Lexicon Pharmaceuticals, Moderna, Neoleukin Therapeutics, Regeneron Pharmaceuticals. BeiGene, a Chinese biotech company, supports unrelated research at the DFCI Translational Immunogenomics Laboratory (TIGL). S.A.C. is a member of the scientific advisory boards of Kymera, PTM BioLabs and Seer and a scientific advisor to Pfizer and Biogen. The remaining authors declare no competing interests.

Additional information

Supplementary information The online version contains supplementary material available at https://doi.org/10.1038/s41586-022-04682-5.

Correspondence and requests for materials should be addressed to Giacomo Oliveira or Catherine J. Wu.

Peer review information *Nature* thanks Jacques Neefjes, Aude Chapuis and the other, anonymous, reviewer(s) for their contribution to the peer review of this work.

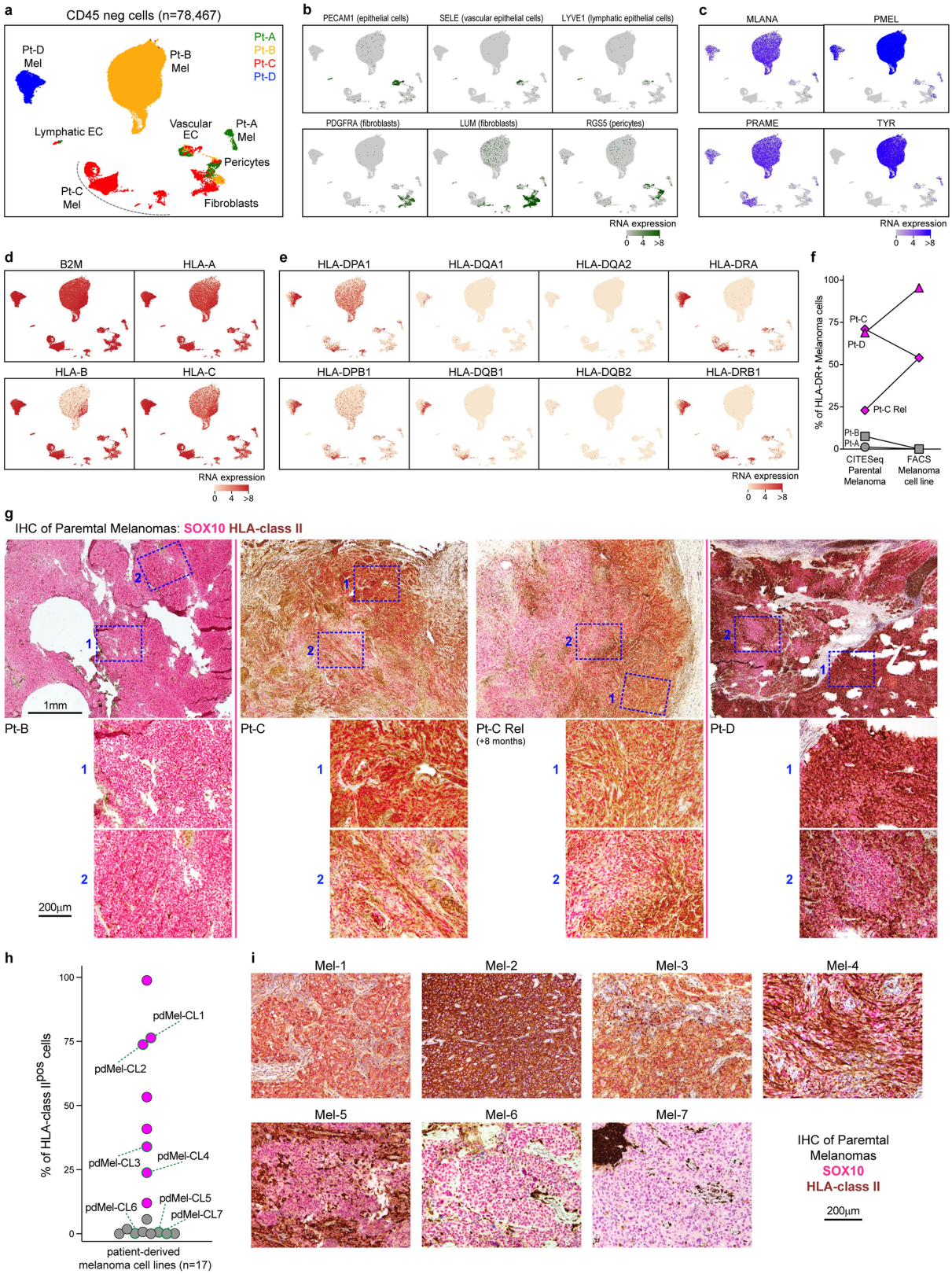

Extended Data Fig. 1 | See next page for caption.

Extended Data Fig. 1 | Characterization of HLA class II expression in melanoma biopsies. a, UMAP of scRNA-seq data from melanoma-enriched $CD45^{neg}$ cells isolated from tumors obtained from 4 patients with melanoma (Pt-A,B,C,D). Patients' origin of cells is denoted with colors. Cell types are inferred based on the expression of markers depicted in panels b-c. EC: endothelial cells. **b**, Single-cell RNA expression of markers associated with non-tumor subpopulations, as reported in[38]. **c**, Single-cell RNA expression of melanoma-associated markers, which allow identification of melanoma cells within patient-specific clusters. **d, e**, Single-cell expression of canonical HLA class I (**d**) and HLA class II (**e**) transcripts, which demonstrate aberrant HLA class II expression in Pt-C and Pt-D parental tumors. **f**, Levels of HLA-DR surface expression detected on melanoma cells from 4 patients of the discovery cohorts (Pt-A,B,C,D, corresponding to different symbol shapes). HLA-DR expression is detected on primary melanoma cells through CITE-seq (left, as shown also in Fig. 1c) and on patient-derived melanoma cell lines through flow cytometry (right). Melanomas are classified in HLA class II^{pos} (magenta) and HLA class II^{neg} (grey). For Pt-C, two primary biopsies (Pt-C and Pt-C Rel) collected longitudinally have been analyzed. **g**, Dual chromogenic immunohistochemical (IHC) staining of formalin-fixed paraffin-embedded (FFPE) tumor samples from Pt-B/C/D for HLA class II (brown) and melanoma transcription factor SOX10 (red-pink). For each specimen, the whole slide was assessed for HLA class II expression. Representative low-magnification images of tumors are provided in top images, with blue boxes identifying representative areas (n = 2 repeated acqusitions), as depicted in bottom panels with 20X magnifications. For Pt-C, the same analysis was performed on 2 tumor biopsies collected at 8 months interval, demonstrating the stability of HLA class II pattern of expression in melanoma cells. **h, i**, Tumor HLA class II expression on independent melanoma specimens (Supplementary Table 3). HLA class II expression was measured by flow cytometry on patient-derived tumor cell lines generated from 17 different patients with melanoma (**h**). Cell lines are classified as HLA class II^{pos} (magenta) and HLA class II^{neg} (grey). For cell lines with available FFPE tissue blocks from parental tumors (Mel-1/7), Dual chromogenic IHC staining was performed (**i**) using HLA class II (brown) and melanoma SOX10 (red-pink) antibodies. For each specimen, the whole slide was assessed for HLA class II expression. Representative images are displayed. The IHC-stainings document patterns of melanoma HLA class II expression similar to what observed in corresponding cell lines, demonstrating that such feature was constitutive and stably perpetuated in culture in the absence of an inflammatory milieu.

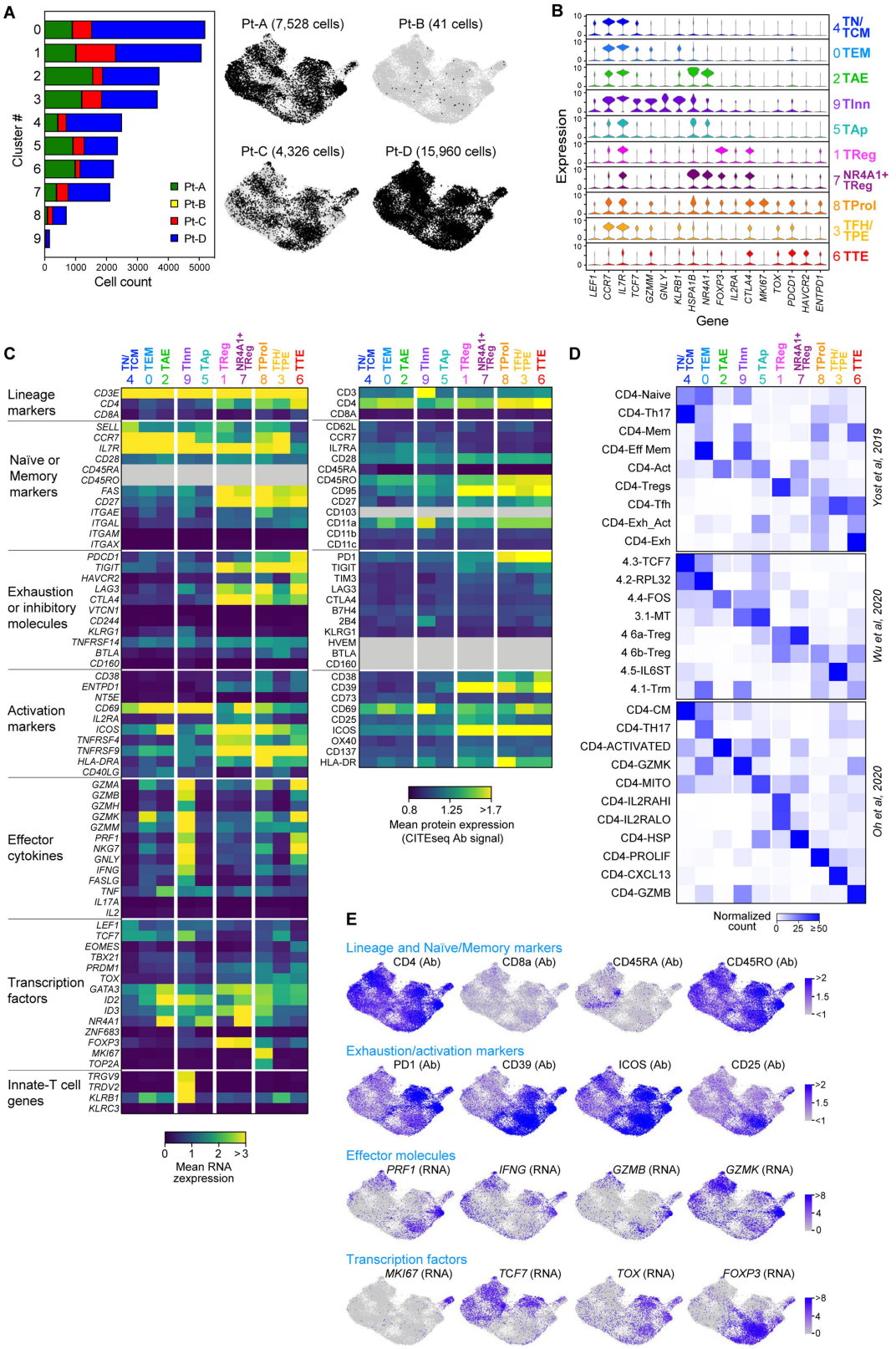

Extended Data Fig. 2 | See next page for caption.

Extended Data Fig. 2 | Single-cell profiling of CD4$^+$ tumor infiltrating lymphocytes. a, Size and patient distribution of the 10 clusters identified from CD4$^+$TIL scRNA-seq. Left: per cluster, patient origin is denoted by color. Right: UMAPs depicting cluster distribution of patient-specific CD4$^+$TILs. **b**, Violin plots quantifying relative transcriptional expression of genes (columns) with high differential expression among CD4$^+$TIL clusters (rows). **c**, Heatmaps depicting the mean cluster expression of a panel of T cell related genes, measured by scRNA-seq (left panel) and the mean surface expression of the corresponding proteins measured through CITE-seq (right panel). Clusters (columns) are labelled using the annotation provided in Fig. 1d; markers (rows) are grouped based on their biological function. Grey - unevaluable markers (CD45 isoforms for scRNA-seq) or which were not assessed (for CITE-seq). CITE-seq CD3 surface expression was poorly detected because of the presence of competing anti-CD3 sorting antibody. **d**, Characterization of the CD4$^+$TIL clusters using independent reference gene-signatures[4–6]. Heatmaps show cross-labelling of T cell clusters defined in the present study (columns, reported as in Fig. 1d) versus reference gene-signatures (rows) derived from the analyses in Yost et al.[4], Wu et al.[5] and Oh et al.[6], with intensities indicating normalized frequency. **e**, UMAPs depicting the single-cell expression of representative T cell markers among CD4+TILs either through detection of surface protein expression with CITE-seq (Ab), or through scRNA-seq (RNA).

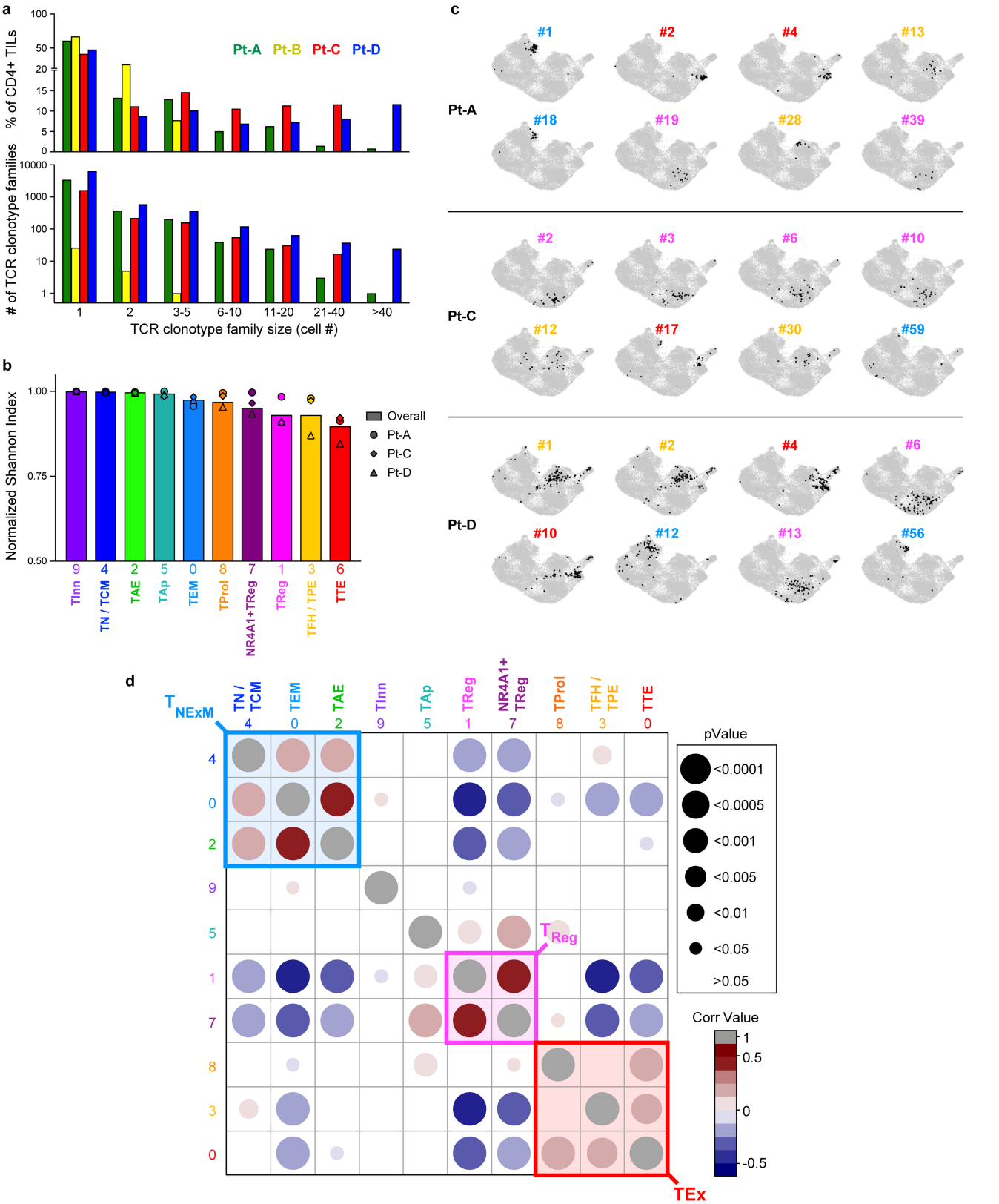

Extended Data Fig. 3 | Clonality of CD4⁺TILs and cell states of TCR clonotypes. a, Histograms depicting the number (bottom panel) and overall frequency (top panel) of patients' TCR clonotype families divided in categories based on their size (x axis). **b**, Histograms showing the intra-cluster TCR clonality, calculated for CD4⁺ T cells in each cluster (x axis) using normalized Shannon index. Symbols - individual TCR clonality for the 3 patients with high numbers of TILs (Pt-A, Pt-C, Pt-D). Bars - the overall TCR clonality measured within each cluster. **c**, UMAPs of the cluster distribution of representative dominant TCR clonotype families among CD4⁺TILs from TIL-rich patients (n = 3). For each patient, numbers denote the ranking of each TCR clonotype (see Fig. 1e), while colors identify their primary cluster (see Fig. 1d). **d**, Matrix displaying Spearman correlation of normalized cluster distribution of dominant TCR clonotype families composed by ≥4 cells. Colors and area of the circles indicate the strength and significance of the correlation, respectively.

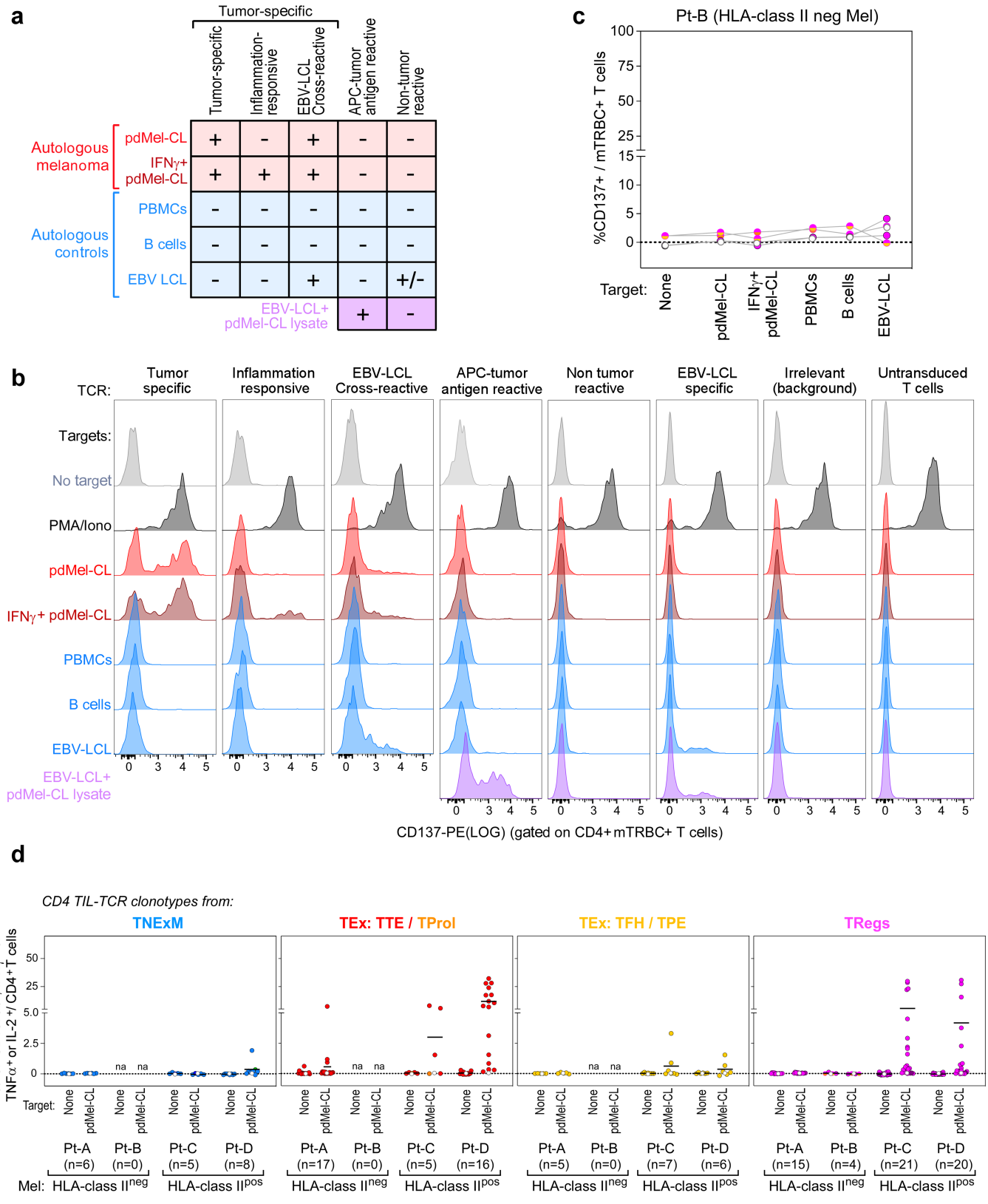

Extended Data Fig. 4 | See next page for caption.

Extended Data Fig. 4 | Antitumor reactivity of *in vitro* reconstructed TCRs. **a**, Schema for classification of TCR reactivities based on CD137 upregulation of TCR transduced T cell lines upon challenge with patient-derived melanoma cells (pdMel-CLs, with or without IFNγ pre-treatment [red]), with controls (PBMCs, B cells and EBV-LCLs [blue]), or with EBV-LCLs pulsed with tumor lysate (purple). **b**, Representative flow cytometry plots depicting CD137 upregulation measured on $CD4^+$ T cells transduced with TCRs isolated from $CD4^+$ melanoma TILs and cultured with melanoma or control targets. Background reactivity was estimated by measuring CD137 upregulation on $CD4^+$ T cells transduced with an irrelevant TCR. **c**, TCR reactivities from Pt-B, measured on TCR transduced ($mTRBC^+$) $CD4^+$ lymphocytes cultured alone or with patient-derived target cells. Background activation measured on $CD4^+$ T cells transduced with an irrelevant TCR was subtracted. Each dot-line set represents the behavior of a single TCR; dot colors denote cell states of TCR clonotypes, as delineated in Fig. 1c; white dots show background signal of untransduced $CD4^+$ T cells. **d**, Cytotoxic potential provided by TCRs isolated from all 4 studied melanoma patients and reconstructed from memory clusters (blue), from T_{TE} and T_{Prol} exhausted clusters (red), from T_{FH}/T_{PE} exhausted clusters (yellow) or from T_{Reg} clusters (magenta). Degranulation ($CD107a/b^+$) and concomitant production of cytokines (IFNγ, TNFα and IL-2) were assessed through intracellular staining, gating on TCR-transduced ($mTRBC^+$) CD4+ T cells cultured alone or in the presence of autologous melanoma (pdMel-CLs). Each dot represents the result for a single TCR isolated from $CD4^+$TILs, color-coded based to its primary phenotypic cluster (as defined in Fig. 1d). For each analyzed TCR, background cytotoxicity from $CD4^+$ T cells transduced with an irrelevant TCR was subtracted. White dots - basal level of activation of untransduced cells. Overall, these data indicate that antitumor cytotoxicity mainly resides among TCR clonotypes with exhausted and regulatory primary clusters.

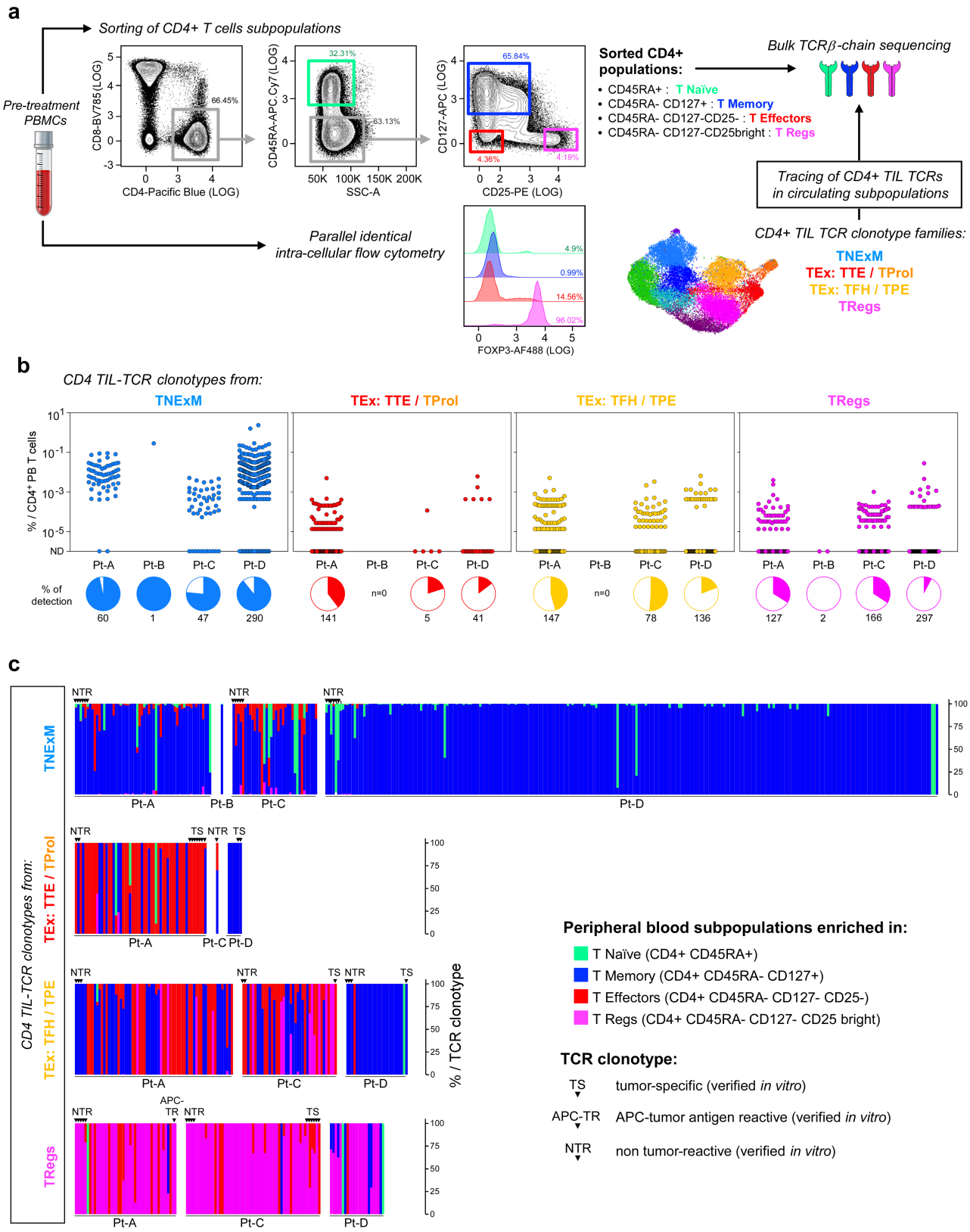

Extended Data Fig. 5 | See next page for caption.

Extended Data Fig. 5 | Peripheral blood phenotype and distribution of CD4+ intratumoral TCR clonotypes. a, Schema for analysis of peripheral blood distribution and phenotype of $CD4^+$ intratumoral clonotypes. PBMCs collected at pre-treatment timepoints from 4 melanoma patients in the discovery cohort were FACS-sorted to isolate $CD4^+$ fractions enriched in T Naïve, T Memory, T Effectors and T Regulatory cells. FACS-plots show the sorting strategy for a representative patient (Pt-A). In parallel, an aliquot of PBMCs was analyzed with intracellular flow-cytometry using the same panel of antibodies with the addition of FOXP3 marker, to confirm enrichment of $FOXP3^+$ cells within the $CD4^+T_{Reg}$ fraction. Bulk sequencing of TCRβ-chains was performed on sorted $CD4^+$ subpopulation to detect the TCRβ-chains of $CD4^+$TIL-TCR clonotype families (with >1 cell). This allowed to trace in the peripheral blood the TCR clonotypes with different intratumoral phenotypes. **b**, Peripheral blood frequencies of $CD4^+$TIL-TCR clonotypes. TCR clonotype families detected amongst $CD4^+$TILs and with different primary clusters (T_{NExM}, T_{Ex}: T_{TE}+T_{Prol}, T_{Ex}: T_{FH}/T_{PE}, T_{Regs}) were traced in peripheral blood, as depicted in **a**. The frequency of each TCR clonotype among circulating $CD4^+$ T cells was reconstructed by taking into account the frequencies of $CD4^+$ subpopulations (determined by FACS-sorting) and the frequencies of each TCRβ-chain within each CD4 fraction (determined by bulk TCRseq). For each patient, the proportion of $CD4^+$TIL-TCRs detected in blood is summarized with pies below each graph. **c**, Peripheral blood phenotype of $CD4^+$TIL TCRs. The graphs show the distribution among 4 FACS-sorted fractions of circulating $CD4^+$ T cells for each $CD4^+$TIL-TCR traced in peripheral blood by bulk TCRseq. The TIL-TCR clonotypes are divided based on their intratumoral primary cluster (rows: T_{NExM}, T_{Ex}: T_{TE}+T_{Prol}, T_{Ex}: T_{FH}/T_{PE}, T_{Regs}) and based on the patient of origin (x axis). TCRβ-chains corresponding to TCR clonotypes reconstructed *in vitro* are pointed with arrows and labeled based on classification of their reactivity as reported in the legend.

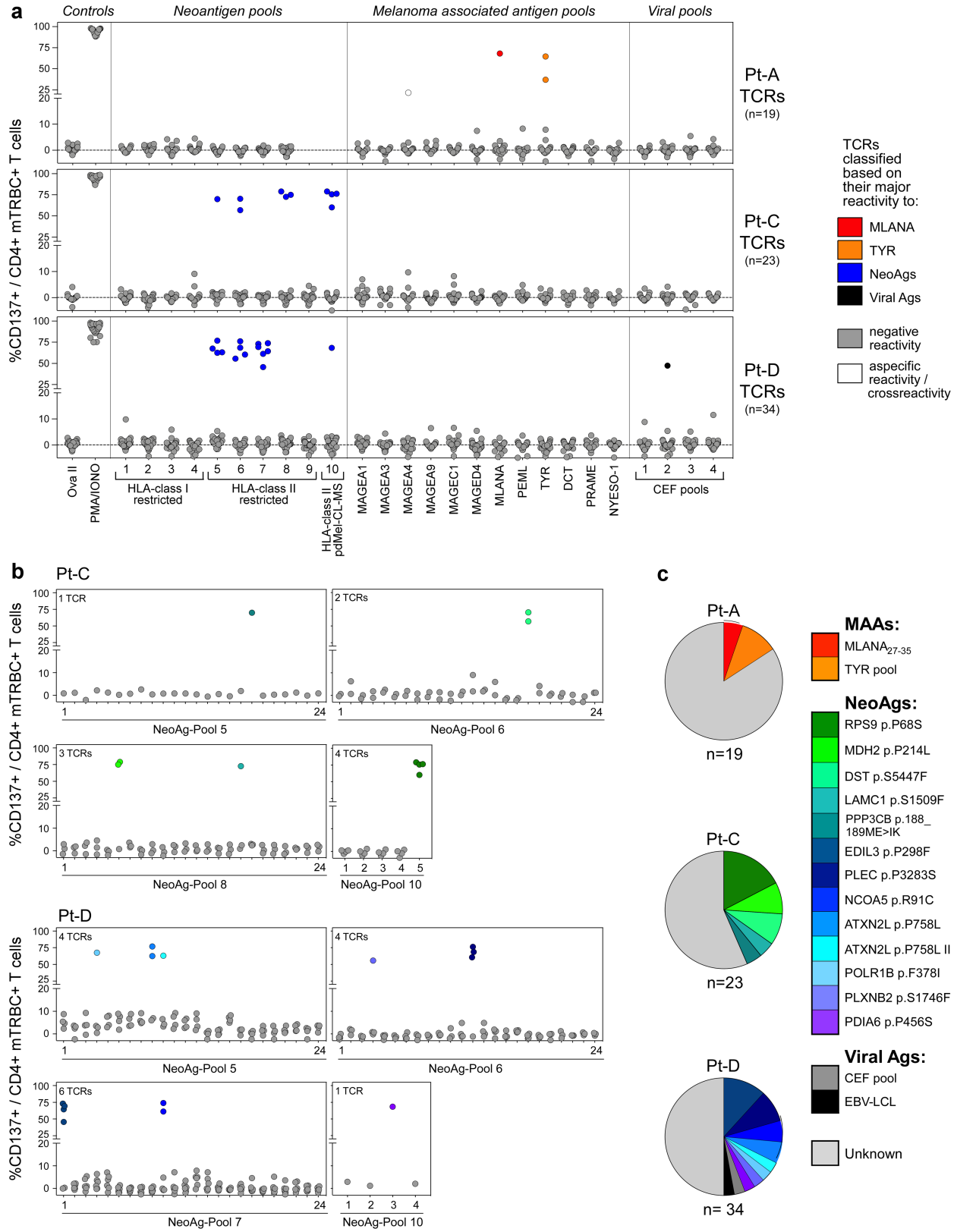

Extended Data Fig. 6 | See next page for caption.

Extended Data Fig. 6 | Antigen specificity of CD4$^+$ tumor-reactive TCRs. **a**, Antigen specificity screening of 76 CD4$^+$TCRs with direct or indirect tumor recognition. Upregulation of CD137 was assessed by flow-cytometry on CD4$^+$ T cells transduced with previously identified tumor-specific or APC-tumor antigen reactive TCRs. Antigen recognition was tested upon culture with autologous EBV-LCLs pulsed with pools of peptides corresponding to immunogenic neoantigens (NeoAgs) predicted to bind patients' HLA class I or II restrictions or detected through Mass-spectrometry (MS) within the HLA class II immunopeptidome (see Supplementary Table 6), known melanoma associated antigens (MAAs) or immunogenic viral epitopes (CEF pools). Reactivity was also assessed against an irrelevant long peptide (Ova II) or in the presence of polyclonal stimulators (PMA/ionomycin) as negative and positive controls, respectively. Background, assessed using DMSO-pulsed target cells, was subtracted from each condition. Colored dots – confirmed antigen-reactive TCRs, colored based on highest reactivity against a particular antigen, as per the legend, compared to the other tested antigens; white dots –TCRs reactive against an antigen which was not the highest of the panel of antigens tested, and hence considered a cross-reactive response; grey dots - negative responses. **b**, Deconvolution of antigen specificity of TCRs reactive to NeoAg-peptide pools. Colored dots indicate the deconvoluted cognate antigens, with antigens corresponding to colors represented in panel **c**. **c**, Distribution of antigen specificities of tumor reactive CD4$^+$TCRs per patient successfully deorphanized after screening. Colors denote the distinct peptides recognized by individual TCRs.

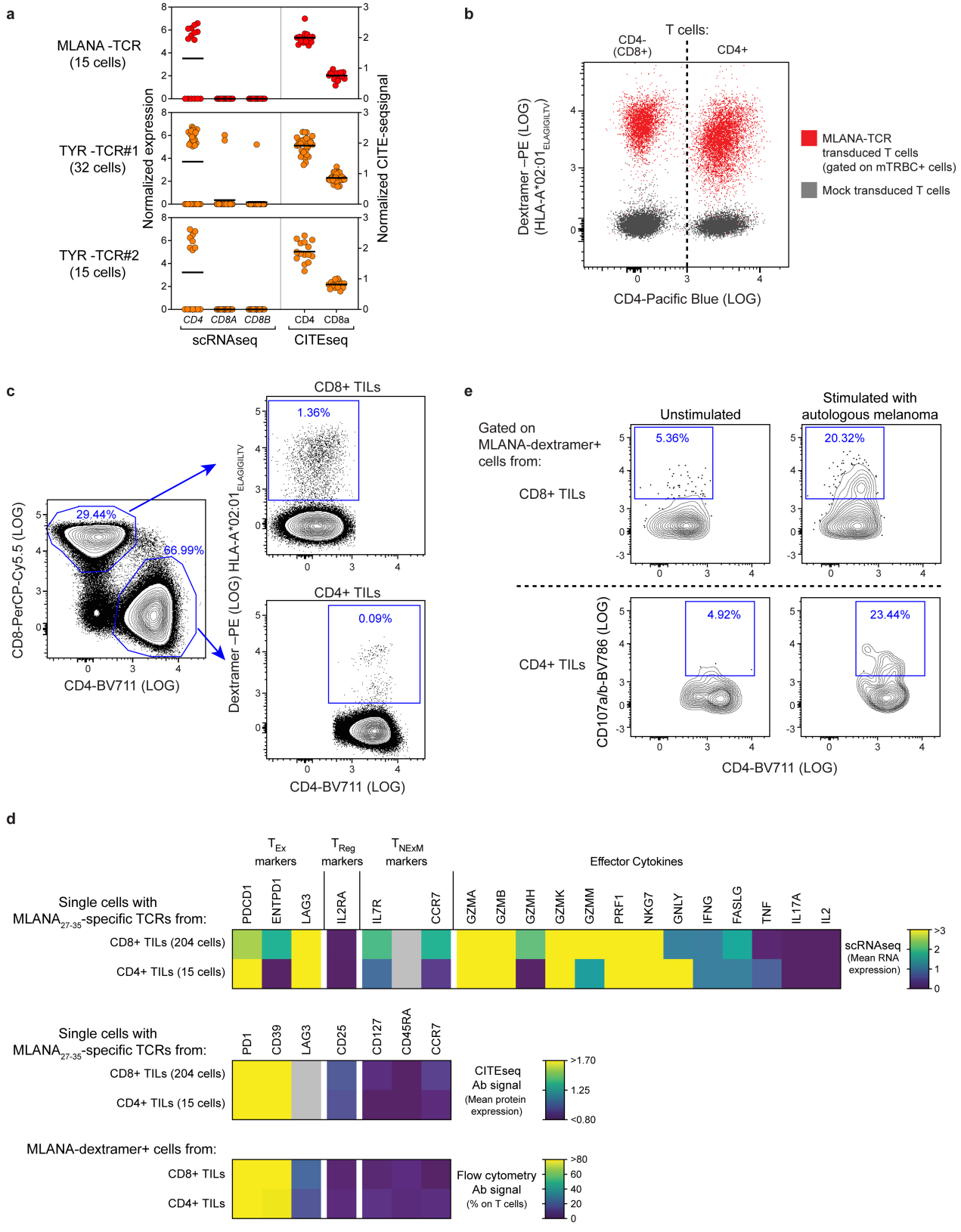

Extended Data Fig. 7 | See next page for caption.

Extended Data Fig. 7 | Characterization of HLA class I restricted CD4$^+$TILs. **a**, Levels of CD4/CD8 transcripts (left, detected by scRNA-seq) or surface proteins (right, detected by CITE-seq) expressed by single cells with CD4$^+$ HLA class I restricted TCRs specific for MLANA (n = 1) or TYR (n = 2) isolated from Pt-A. The data indicate that the 3 clonotype families belong to CD4$^+$TILs, despite their reactivity to HLA class I restricted epitopes. **b**, Flow cytometric plot depicting peptide-HLA binding of T cells transduced with MLANA$_{27\text{-}35}$-specific TCR (red), isolated in CD4$^+$TILs from Pt-A. Transduced T cells comprising CD4$^+$ and CD8$^+$ (CD4$^-$) lymphocytes were stained using HLA-A*02:01 dextramers loaded with MLANA$_{26\text{-}35}$ heteroclitic peptide (ELAGIGILTV). Untransduced T cells (grey) are shown as control. The similar level of binding exhibited by CD4+ and CD8+ T cells demonstrates that tested HLA class I TCR act independently from CD4/CD8 co-stimulation. **c**, Flow cytometry tracing of MLANA-specific HLA class I restricted CD4$^+$ T cells in Pt-A TILs. Plots depict identification of CD4$^+$ or CD8$^+$ cells within CD3$^+$ TILs from Pt-A (left) and binding to HLA-A*02:01 dextramers loaded with MLANA$_{26\text{-}35}$ heteroclitic peptide among CD4$^+$ or CD8$^+$ TILs (right). Frequencies of each population are provided (blue), demonstrating reliable detected of HLA class I restricted CD4$^+$TILs. **d**, Phenotype of MLANA-specific HLA class I restricted CD4$^+$TILs from Pt-A. Heatmaps show transcript levels detected by scRNA-seq (top), surface protein expression measured by CITE-seq (middle) or flowcytometry (bottom) for CD4$^+$ T cells with TCRs specific for HLA-A*02:01-MLANA$_{26/27\text{-}35}$ complexes. As comparison, the same analysis was performed on CD8$^+$ TILs specific for the same antigen-HLA (as identified in[13]) or detected by flow cytometry (as depicted in panel **c**). Markers detected with all the 3 technologies are shown (exhaustion markers: PD-1, CD39, LAG3; regulatory marker: CD25; memory markers: CD127, CD45RA, CD127). For scRNA-seq (top) transcripts related to effector molecules are reported. Grey color: values not available. This analysis shows that HLA class I restricted CD4$^+$TILs specific for MLANA display an exhausted and cytotoxic phenotype similar to the one of CD8$^+$ TILs. **e**, Cytotoxicity of HLA-class I-restricted CD4$^+$TILs. Degranulation (CD107a/b upregulation) measured *in vitro* on MLANA-specific HLA-A*01:02 restricted CD4$^+$ or CD8$^+$ T cells, identified in TILs from Pt-A as depicted in **c**. Cells were cultured in the absence (left) or presence (right) of autologous melanoma for 6 h. HLA-class I restricted CD4$^+$TILs specific for MLANA antigen (bottom raw) exhibited degranulation levels comparable to those observed for CD8$^+$ counterparts (top raw), demonstrating their ability to mediate cytotoxicity.

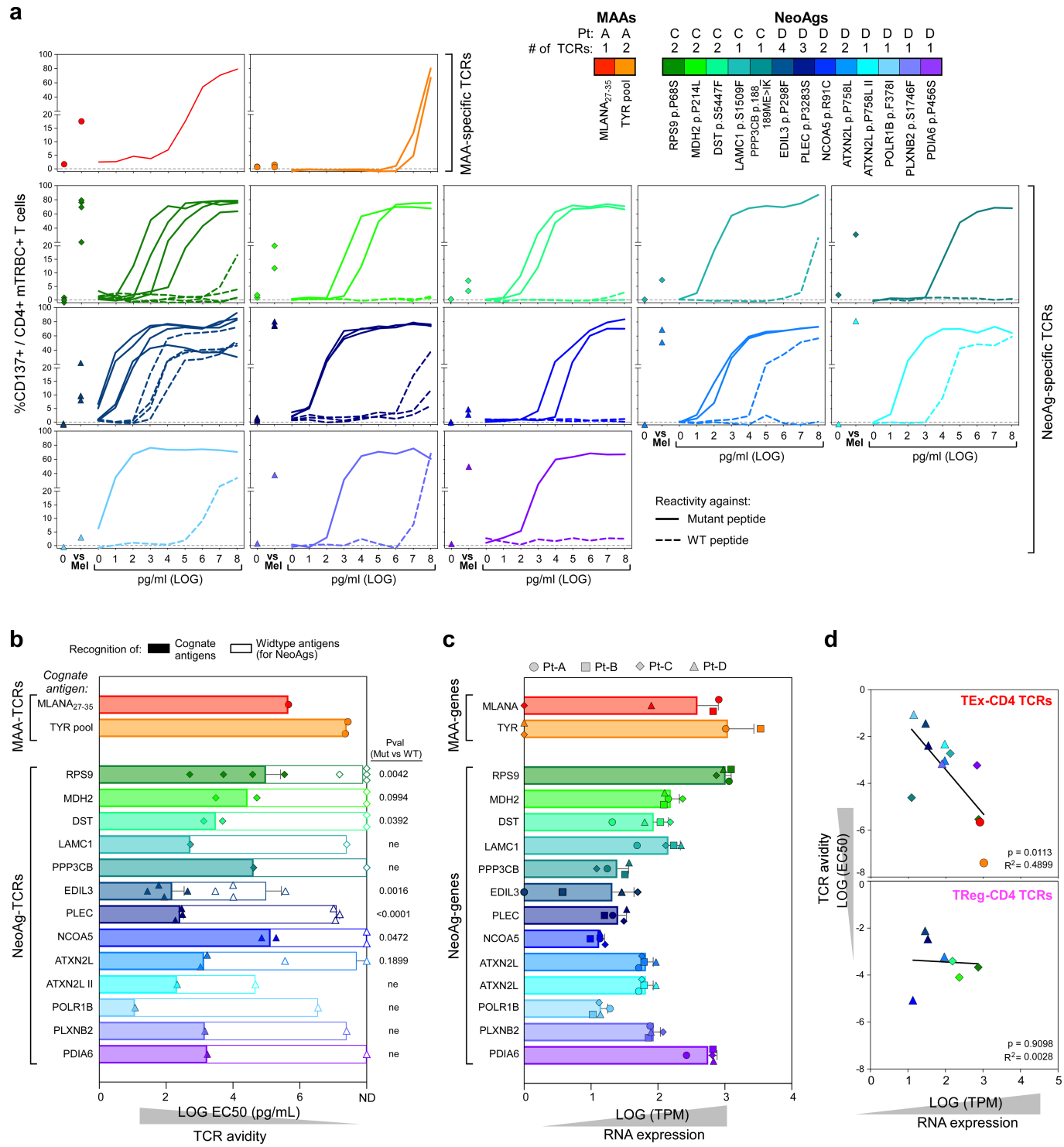

Extended Data Fig. 8 | See next page for caption.

Extended Data Fig. 8 | Avidities of CD4$^+$ MAA/NeoAg-TCRs. a, Avidity of de-orphanized TCRs with MAA or NeoAg specificity (n = 3 and n = 23 respectively). TCR-dependent CD137 upregulation was measured on TCR-transduced (mTRBC$^+$) CD4$^+$ cells upon culture with patient-derived EBV-LCLs pulsed with increasing concentrations of the cognate antigen (MAAs in the top panels, NeoAgs in bottom panels). Background activation measured on CD4$^+$ T cells transduced with an irrelevant TCR was subtracted. Reactivity to DMSO-pulsed targets (0) and autologous melanoma (pdMel-CL) are reported on the left; for NeoAg-specific TCRs, the dashed lines report reactivity against wildtype peptides. A color legend depicts the different cognate antigens targeted by the deorphanized TCRs and specifies the number of TCRs able to recognize each cognate antigen and the patient the TCR belongs to. **b**, EC50 calculated from titration curves of MAA or NeoAg-specific TCRs (n = 3 and n = 23 respectively); note that high EC50 values correspond to low TCR avidities. Means with SD are reported, with TCR numbers corresponding to those reported in **a**. **c**, Expression levels of MAA or NeoAg transcripts (from bulk RNAseq of pdMel-CLs) from which the analyzed epitopes are generated, as a measure of cognate peptide abundance in tumor cells. Columns show means values with s.d. of values from n = 4 pdMel-CLs (symbols). **d**, Correlation between the avidity of antitumor CD4$^+$TCRs (y axis) and target abundance (x axis), as measured by RNA expression of TCR-targeted genes detected in the autologous pdMel-CLs and expressed as transcripts per million mapped reads (TPM). Values for TCR avidity represent averages of EC50 data presented in **b**. The correlation is measured on de-orphanized antitumor CD4$^+$TCR specificities with intratumoral T_{Ex} (top) or T_{Reg} (bottom) primary clusters, as showed in Fig. 3b, f. Significance of each linear regression is reported within each panel. Symbols: patients from whom TCRs were identified. Colors: cognate antigens of antitumor TCRs, as depicted in **a**.

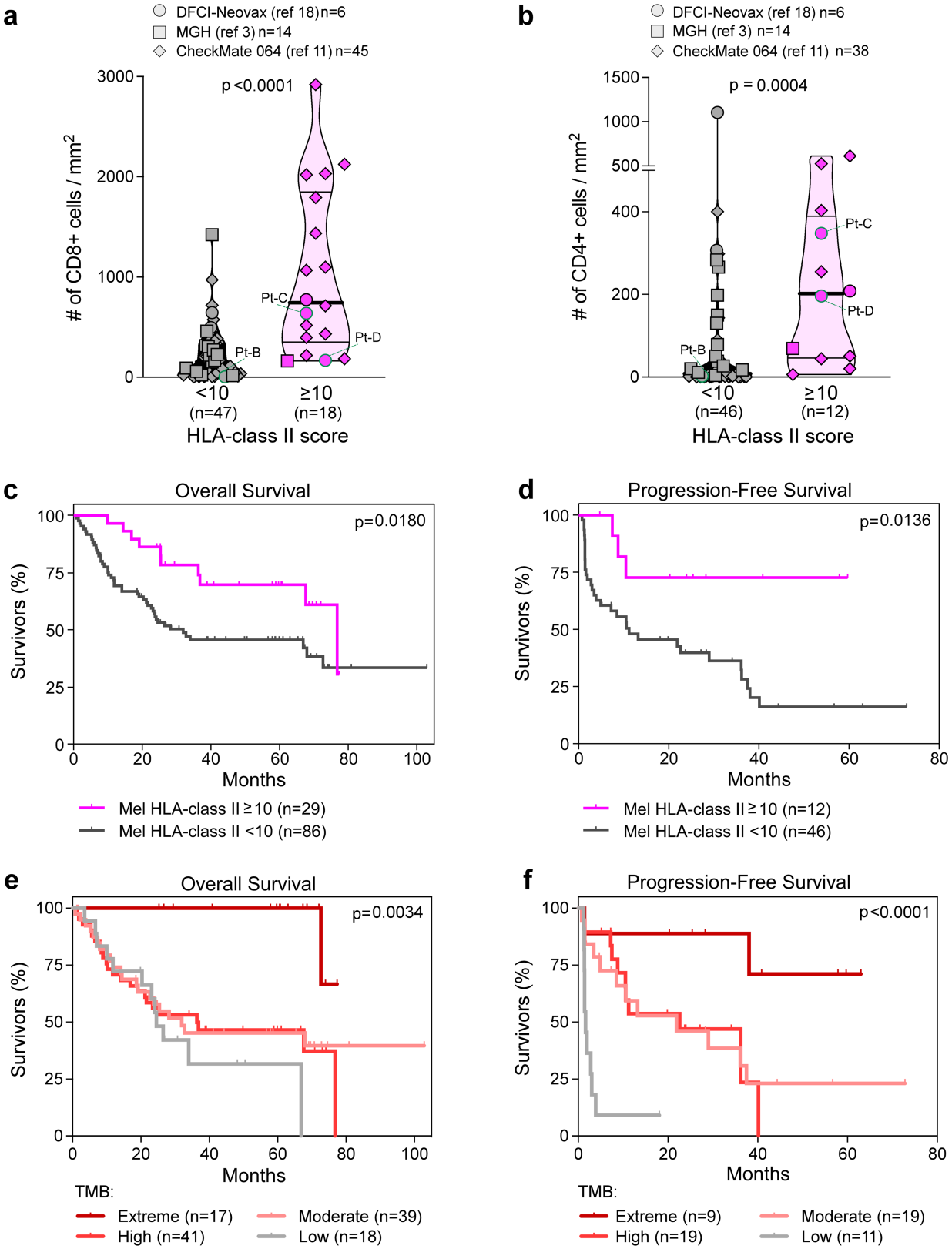

Extended Data Fig. 9 | See next page for caption.

Extended Data Fig. 9 | Quantification of TILs and clinical outcome of patients with melanoma. a, b, Quantification of $CD8^+$ (**a**) and $CD4^+$ (**b**) TILs detected in tumor specimens from patients reported in cohorts from published studies[3,11,18]. TILs were quantified in tumor areas using immunohistochemical or immunofluorescence stainings (see Supplementary Information). Only patients with available tumor FFPE were analyzed (n indicated in the legends). Values from patients included in the discovery cohort are labeled (specimens from Pt-A were not available for this analysis). Melanoma were classified based on HLA class II expression, scored on tumor cells by IHC (≥ or < 10% of tumor cells with positive staining). Patients from each study are denoted by different symbol shapes (as reported in each legend, with number of patients for each cohort). Horizontal lines show median (bold) and quartiles values; p-values indicate the significance of comparisons calculated using Mann-Whitney test. **c**–**f**, Clinical outcome of patients with melanoma, classified based on tumor HLA class II expression (**c, d**) or based on classes of tumor mutation burden (**e, f**), as defined in Fig. 4a and indicated in each color legend. Kaplan-Meier curves estimate the overall survival (**c, e**) and progression-free survival (**d, f**) of patients with melanoma from 4 published studies[3,11,18,19]. Only patients with available overall survival or progression-free survival after treatment with immunotherapies have been analyzed (see Supplementary Table 8). For each category, number of analyzed patients is reported within the legends. P-values indicate the significance of comparison between Kaplan-Meier curves, as obtained using Log-rank Mantel-Cox test between 2 groups (**c, d**) or 4 groups (**e, f**).

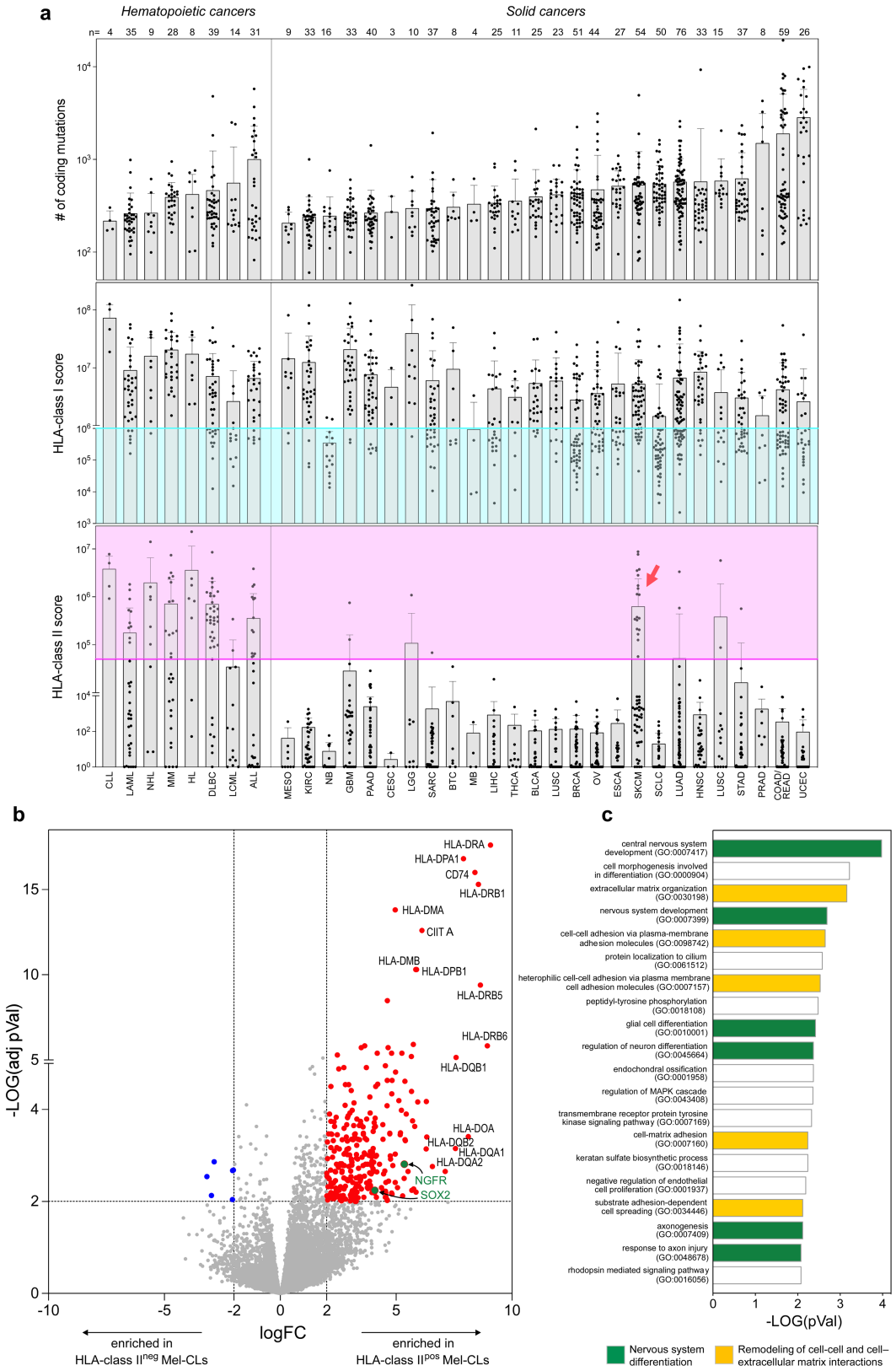

Extended Data Fig. 10 | See next page for caption.

Extended Data Fig. 10 | Analysis of HLA class II expression in cancer cell lines. a, Tumor mutation burden (top panel) with HLA class I and HLA class II expression scores (middle and bottom panels) of 927 human cancer cell lines[22]. HLA class I and II scores have been calculated from RNAseq as described in the Material and Methods section. Colored areas denote downregulation of HLA class I (turquoise) and upregulation of HLA class II (pink). Each tumor type is indicated using the corresponding abbreviation from TCGA (x axis). The number of tested cancer cell lines for each tumor type is reported (top). Bars depict mean values with s.d. Compared to hematopoietic tumors, melanoma (SKCM) represents the sole solid cancer with a relevant number of HLA class II^{pos} cell lines (red arrow). **b**, Volcano plot showing RNA transcripts deregulated upon comparison of HLA class II^{pos} (n = 18) and HLA class II^{neg} (n = 36) melanoma cell lines (Mel-CLs). Significantly upregulated or downregulated genes ($log_2FC \geq 2$ or $log_2FC \leq -2$, adj-p.value ≤ 0.01) are colored in red or blue respectively. HLA class II related genes are labeled; Upregulated genes previously associated with de-differentiated melanoma[23,24,47] are highlighted in green. **c**, Top 20 gene ontology processes enriched in transcripts upregulated in HLA class II^{pos} Mel-CLs. HLA class II related genes were excluded from this analysis. Bars depict enrichment, as calculated using two-sided Fisher's exact test[48]. Processes related to differentiation of central nervous system are colored in green, while processes related to remodeling of interactions with cells or extracellular matrix are highlighted in yellow. Enrichment in such gene-ontologies, characteristic of neural-crest-like tumors[23,24,47], in HLA class II^{pos} melanoma confirm that HLA class II expression is peculiar of de-differentiated melanoma. No significant deregulation of genes derived from HLA class II RNA-interference screens[49] was observed.

nature research

Corresponding author(s): Giacomo Oliveira
giacomo_oliveira@dfci.harvard.edu
Catherine J. Wu cwu@partners.org

Last updated by author(s): Mar 4, 2021

Reporting Summary

Nature Research wishes to improve the reproducibility of the work that we publish. This form provides structure for consistency and transparency in reporting. For further information on Nature Research policies, see our Editorial Policies and the Editorial Policy Checklist.

Statistics

For all statistical analyses, confirm that the following items are present in the figure legend, table legend, main text, or Methods section.

n/a	Confirmed	
☐	☒	The exact sample size (*n*) for each experimental group/condition, given as a discrete number and unit of measurement
☐	☒	A statement on whether measurements were taken from distinct samples or whether the same sample was measured repeatedly
☐	☒	The statistical test(s) used AND whether they are one- or two-sided *Only common tests should be described solely by name; describe more complex techniques in the Methods section.*
☒	☐	A description of all covariates tested
☐	☒	A description of any assumptions or corrections, such as tests of normality and adjustment for multiple comparisons
☐	☒	A full description of the statistical parameters including central tendency (e.g. means) or other basic estimates (e.g. regression coefficient) AND variation (e.g. standard deviation) or associated estimates of uncertainty (e.g. confidence intervals)
☐	☒	For null hypothesis testing, the test statistic (e.g. *F*, *t*, *r*) with confidence intervals, effect sizes, degrees of freedom and *P* value noted *Give P values as exact values whenever suitable.*
☒	☐	For Bayesian analysis, information on the choice of priors and Markov chain Monte Carlo settings
☒	☐	For hierarchical and complex designs, identification of the appropriate level for tests and full reporting of outcomes
☒	☐	Estimates of effect sizes (e.g. Cohen's *d*, Pearson's *r*), indicating how they were calculated

Our web collection on statistics for biologists contains articles on many of the points above.

Software and code

Policy information about availability of computer code

Data collection	All single-cell sequencing data were processed with Cell Ranger software (version 3.1.0). Bulk TCR or RNA sequencing were processed as described in Li et al. Nat Protoc 2019
Data analysis	Data were analyzed using R version 3.6.3, and the following packages and versions in R for analysis: Broad Picard Pipeline (WES/RNA-seq), GATK4 v4.0, Mutect2 v2.7.0 (SNV and indel identification), NetMHCpan 4.0 and NetMHCIIpan 4.0(neoantigen binding prediction), ContEst v1 (contamination estimation), ABSOLUTE v1.1 (purity/ploidy estimation), STAR v2.6.1c (sequencing alignment), RSEM v1.3.1 (gene expression quantification), Seurat v3.2.0 (single-cell sequencing analysis), Harmony v1.0 (single-cell data normalization), SingleR v3.22 (scater package), Scanpy v1.5.1, Python v3.7.4 (for comparison with other single cell datasets), EdgeR (to compare bulk RNAseq expression), EnrichR (to analyze enrichment of gene ontologies). Flow cytometry data were analyzed with Flowjo v 10.3 and FACSDiva v8.0.1 and figures with statistich were generated through GraphPad Prism 9 or R . Computer code used to generate the analyses is available at https://github.com/kstromhaug/oliveira-stromhaug-cd4-code.

For manuscripts utilizing custom algorithms or software that are central to the research but not yet described in published literature, software must be made available to editors and reviewers. We strongly encourage code deposition in a community repository (e.g. GitHub). See the Nature Research guidelines for submitting code & software for further information.

Data

Policy information about availability of data

All manuscripts must include a data availability statement. This statement should provide the following information, where applicable:

- Accession codes, unique identifiers, or web links for publicly available datasets
- A list of figures that have associated raw data
- A description of any restrictions on data availability

SSingle-cell RNA, TCR and CITEseq sequencing are available through dbGaP portal (study Id 26121, accession number phs001451.v3.p1). Previously published scRNA-seq, scTCR-seq and bulk TCR-seq data reanalyzed here are available from gene expression omnibus under accession codes GSE123814 (Yost et al, Net Med 2019), GSE139555 (Wu et al, Nature 2020), GSE149652 (Oh et al, Cell 2020) or from portal www.broadinstitute.org/ccle (Ghandi et al, Nature 2019). All other data and codes are presented in the main text or in the supplementary materials and are available from the corresponding authors upon reasonable request.

Field-specific reporting

Please select the one below that is the best fit for your research. If you are not sure, read the appropriate sections before making your selection.

☒ Life sciences ☐ Behavioural & social sciences ☐ Ecological, evolutionary & environmental sciences

For a reference copy of the document with all sections, see nature.com/documents/nr-reporting-summary-flat.pdf

Life sciences study design

All studies must disclose on these points even when the disclosure is negative.

Sample size

To investigate the lansdscape of CD4+ T cells with single-cell profiling, sample size of patients was determined by the availability of tumor specimens and reliable patient-derived melanoma cell lines. We focused our investigations on 4 melanoma patients (discovery cohort) whose tumors were previously genomically characterized [Ott, 2017; Hu,Leet 2021, Oliveira, 2021]. Only for these subjects a sufficient amount of autologous melanoma cells were available to screen the antitumor potential of TCRs. Moreover, current technologies pose a limit to the number of TCRs that can be reconstructed and screened, and therefore we studied the properties of a relevant number of TCRs in a small cohort of patients.

To achieve a detailed description of intratumoral cell states, the amount of single cells sequenced from TILs was dramatically increase by performing repeated measurement of the same tumor specimens. This allowed to retrieve a number of CD4+ cells that is comparable to other published dataset, but with an unprecedented level of detail for each individual specimen. No sample size calculation was performed; number of repeated single-cell acquisitions was limited by availability of cells and costs, and hence up to 4 acuisition were performed per sample. These experiments resulted in the sequencing of a number of CD4+ T cells per patients that was from 50 to 100 times superior to what reported in external datasets of melanoma TILs (Sade-Feldman et at, Cell 2019; Li et al, Cell 2019; Jerby-Arnon et al, Cell 2018, TIrosh et al, Science 2016).

In vitro TCR reconstruction and antigen specificity screening was performed for TCRs from CD4+ TILs of the discovery cohort, selected to be highly expanded within the intratumoral microenvironment or having a primary phenotype representative of all the clusters classified as TEx, TNExM or TReg. Selection criteria also included: i) the availability of reliable sequences for both TCRalpha and TCRbeta chains; ii) the absence of the tested TCRalpha/beta pairs among CD8+ TILs19; iii) the absence of multiple TCRalpha or TCRbeta chains. No sample size calculation was performed; the total number of tested TCRs was mainly limited by experimental costs. TCRs were selected with the aim of describing the behaviour and antigen specificity of TILs from all the identified primary clusters (TNExM, Tex, TReg). At least 5 TCRs per phenotypic compartment were studied for Pt-A, Pt-C, Pt-D: this allowed the description if a sufficiently large portion of CD4+ TILs (>10% of all CD4+ cells), which was superior to any other published study analyzing the specificty of CD4+ TILs.

Stability of HLA-class II expression was validated on patient-derived melanoma cell lines generated from 17 independent treatment-naive melanomas (see Supplementary Table 3). For patients with available parental tumor tissue blocks (n=7), IHC was performed.

Association between tumor HLA-class II expression and tumor mutation burden were invastigate for all the patients with melanoma reported in 4 previous publications (DFCI-Neovax cohort: Hu, Nat Med 2021; MGH cohort: Sade-Feldman, Cell 2019; ChecheMate 064 cohort: Rodig, Sci Transl Med 2018, CheckMate 068 cohort: Anagnostou, Cell Rep Med 2020), with available tumor immunohistochemistry (to detect tumor HLA expression) and WES/RNAseq (to determined tumor mutation burden).

Quantification of TILs through immunohistochemistry or immunofluorescence was possible for tumors with available FFPE materials.

Data exclusions

Because of the low number of CD4+ TCR clonotypes detected within the tumor, Pt-B was not included in experiments for TCR antigen specificity screening. In such case, the low number of expanded TCRs available from single-cell sequencing determined the reconstruction of less than 10 TCRs (4 TCRs for Pt-B, Entended Data Fig. 4e); as a results, experiments of antigen specificity screening were estimated to be too costly. For these reasons Pt-B was not included in experiments depicted in Fig. 2, Fig 3 and Extended Data Fig 6.

Replication

Single-cell sequencing of TILs was repeated from 2 to 4 times per tumor specimen, to reach a high number of sequenced CD4+ TILs.

Every TCR selected for functional analysis was tested for reactivity against autologous tumor material at least thrice. TCRs are presented as tumor-reactive only if they demonstrated reactivity to tumor in replicate experiments. All the repeated experiments were successful and equally reliable. Realibility of TCR reconstruction and screening was assessed by including a TCR with know antigen specificity among

experiments. Moreover, positive and negative controls were established (unstimulated: negative controls; policlonal stimulation: positive controls).

For FACS analysis of HLA-class I restricted specificities, reliability of experiments was also assessed by performing control analysis on CD8+TILs. When the amount of viable cells allowed the analysis of multiple aliquots, replicates were performed and always proved consistent results.

Randomization

For each tumor sample analyzed, we selected up to 50TCRs based on their representation within the exhausted, non exhausted or Treg compartment. The amount of tested TCRs was mainly determined by the high cost of TCR reconstruction technologies. The experiments were not randomized and investigators were not blinded to allocation during experiments. Criteria of TCR selectio are described above.

When we analyzed the correlation between HLA expression and tumor mutation burden in 116 patients, melanomas were divided based on the level of HLA-class II expression on tumor: HLA-class IIneg (score<10) or HLA-class IIpos (score >=10). A score corresponding to 10% identified the minimal level of HLA-class II expression that could be detected by IHC. Similarly, melanomas were divided base on the number of coding mutations in parental: low <15th percentile; moderate 15th percentile -median; high median-85th percentile; extreme >85th percentile. The 15th percentile was selected to grant the identification of a subpopulation with extreme TMB, but p with sufficient number of observed melanomas (>10%).

Blinding

No experimental groups were employed in this work, and blinding was therefore not possible nor relevant.

Reporting for specific materials, systems and methods

We require information from authors about some types of materials, experimental systems and methods used in many studies. Here, indicate whether each material, system or method listed is relevant to your study. If you are not sure if a list item applies to your research, read the appropriate section before selecting a response.

Materials & experimental systems

n/a	Involved in the study
☐	☒ Antibodies
☐	☒ Eukaryotic cell lines
☒	☐ Palaeontology and archaeology
☒	☐ Animals and other organisms
☐	☒ Human research participants
☐	☒ Clinical data
☒	☐ Dual use research of concern

Methods

n/a	Involved in the study
☒	☐ ChIP-seq
☐	☒ Flow cytometry
☒	☐ MRI-based neuroimaging

Antibodies

Antibodies used

Flow cytometry antibodies:
anti-human CD45 (PE-Cy7, clone 2D1, Biolegend, catalog # 368532, dilution 1:50)
anti-human CD3 (APC-Cy7, clone UCHT1, Biolegend, catalog # 300426 dilution 1:50)
anti-human CD3 (PE-Cy7, clone UCHT1, Biolegend, catalog # 300420 dilution 1:50)
anti-human CD3 (BV650, clone OKT3, Biolegend, catalog # 317324, dilution 1:30)
anti-human CD3 (R718, clone UCHT1, BD Biosciences, catalog # 566953, dilution 1:50)
anti-human CD4 (Pacific Blue, clone OKT4, Biolegend, catalog # 317424, dilution 1:30)
anti-human CD4 (BV711, clone OKT4, Biolegend, catalog # 317440, dilution 1:50)
anti-human CD8a (BV785, clone RPA-T8, Biolegend, catalog # 301046, dilution 1:100)
anti-human CD8a (PerCP-Cy5.5, clone RPA-T8, Biolegend, catalog # 301032, dilution 1:50)
anti-human CD137 (PE, clone 4B4-1, Biolegend, catalog # 309804, dilution 1:50)
anti-human CD107a (FITC, clones H4A3, Biolegend, catalog # 328606, dilution 1:100)
anti-human CD107a (BV786, clones H4A3, BD Biosciences, catalog # 563869, dilution 1:50)
anti-human CD107b (FITC, clones H4A3, Biolegend, catalog # 354306, dilution 1:100)
anti-human CD107b (BV786, clones H4A3, BD Biosciences, catalog # 565304, dilution 1:50)
anti-human CD45RA (APC-Cy7, clone HI100, Biolegend, catalog # 304128, dilution 1:50)
anti-human CD25 (PE, clone M-A251, Biolegend, catalog # 356104, dilution 1:50)
anti-human CD25 (BV510, clone BC96, Biolegend, catalog # 302640, dilution 1:50)
anti-human CD39 (BV785, clone A1, Biolegend, catalog # 328240, dilution 1:50)
anti-human CD127 (APC, clone A019D5, Biolegend, catalog # 351316, dilution 1:50)
anti-human CD127 (BV650, clone A019D5, Biolegend, catalog # 351326, dilution 1:50)
anti-human CCR7 (BV421, clone G043H7, Biolegend, catalog # 353208, dilution 1:50)
anti-human FOXP3 (AF488, clone 206D, Biolegend, catalog # 320112, dilution 1:50)
anti-human LAG3 (BV605, clone 11C3C65, Biolegend, catalog # 369324, dilution 1:50)
anti-human PD-1 (PE-Cy7, clone EH12.2H7, Biolegend, catalog # 329918, dilution 1:50)
anti-human IFNg (APC-Cy7, clone B27, Biolegend, catalog # 506524, dilution 1:30)
anti-human TNFa (PE-Cy7, clone Mab11, Biolegend, catalog # 502930, dilution 1:100)
anti-human IL-2 (APC, clone MQ1-17H12, eBioscience, catalog # 17-7029-82, dilution 1:100)
anti-mTCRB antibody (PE, clone H57-597, eBioscience, catalog # 12-5961-82, dilution 1:50)
anti-mTCRB antibody (PE-Cy7, clone H57-597, eBioscience, catalog # 25-5961-82, dilution 1:50)
anti-human Fibroblast Antigen (FITC, clone REA165, Miltenyi Biotec, catalog # 130-100-134, dilution 1:20)
anti-human MCSP/HNG2 (PE, clone LHM-2, R&D Systems, catalog # FAB2585P, dilution 1:20)

anti-human HLA-DR,DP,DQ (FITC, clone Tü39, Biolegend, catalog #555558, dilution 1:50)
anti-human HLADR (FITC, clone L243, Biolegend, catalog # 980402, dilution 1:50)
Isotype IgG2b (FITC, clone MPC-11, Biolegend, catalog # 982102, dilution 1:50-1:20)
Isotype IgG1 (FITC, clone G0114F7, Biolegend, catalog # 401914, dilution 1:50-1:20)
Isotype IgG1 (PE, clone G0114F7, Biolegend, catalog # 401906, dilution 1:50-1:20)

HLA-A*02:01 dextramers with MLANA26-35 heteroclitic peptide (ELAGIGILTV) (PE, Immudex, catalog # WB216, dilution 1:20)

Blocking antibodies:
TruStain FcX™ (clone 93, Biolegend, catalog # 101320)

Viability dyes:
Zombie Aqua (Biolegend, catalog# 423102, dilution 1:40)
Zombie Red (Biolegend, catalog# 423110, dilution 1:40)

CITESeq antibodies (all TotalSeqTM-C antibodies from Biolegend)
IgG1 isotype (clone MOPC-21, catalog # 400187)
IgG2a isotype (clone MOPC-173 , catalog # 400293)
IgG2b isotype (clone MPC-11, catalog # 400381)
anti-human B2m (clone 2M2, catalog # 316323)
anti-human B7H4 (clone MIH43, catalog # 358116)
anti-human CD10 (clone HI10a, catalog # 312233)
anti-human CD117 (clone 104D2, catalog # 313243)
anti-human CD11a (clone TS2/4, catalog # 350617)
anti-human CD11b (clone ICRF44, catalog # 301359)
anti-human CD11c (clone S-HCL-3, catalog # 371521)
anti-human CD127 (IL7RA) (clone A019D5, catalog # 351356)
anti-human CD134 (OX40) (clone Ber-ACT35 (ACT35), catalog # 350035)
anti-human CD137 (41BB) (clone 4B4-1, catalog # 309839)
anti-human CD138 (clone DL-101, catalog # 356539)
anti-human CD14 (clone M5E2, catalog # 301859)
anti-human CD15 (clone W6D3, catalog # 323053)
anti-human CD152 (CTLA4) (clone BNI3, catalog # 369621)
anti-human CD16 (clone 3G8, catalog # 302065)
anti-human CD163 (clone GHI/61, catalog # 33363)
anti-human CD18 (clone TS1/18 , catalog # 302129)
anti-human CD183 (CXCR3) (clone G025H7, catalog # 353747)
anti-human CD184 (CXCR4) (clone 12G5, catalog # 306533)
anti-human CD19 (clone HIB19, catalog # 302265)
anti-human CD194 (CCR4) (clone L291H4, catalog # 359425)
anti-human CD197 (CCR7) (clone G043H7, catalog # 353251)
anti-human CD1c (clone L161, catalog # 331547)
anti-human CD1d (clone 51.1, catalog # 350319)
anti-human CD20 (clone 2H7, catalog # 302363)
anti-human CD223 (LAG3) (clone 11C3C65, catalog # 369335)
anti-human CD226 (DNAM-1) (clone 11A8, catalog # 338337)
anti-human CD244 (2B4) (clone C1.7, catalog # 329529)
anti-human CD25 (clone BC96, catalog # 302649)
anti-human CD27 (clone O323, catalog # 302853)
anti-human CD274 (PDL1) (clone 29E.2A3, catalog # 329751)
anti-human CD278 (ICOS) (clone C398.4A, catalog # 313553)
anti-human CD279 (PD1) (clone EH12.2H7, catalog # 329963)
anti-human CD28 (clone CD28.2, catalog # 302963)
anti-human CD3 (clone UCHT1, catalog # 300479)
anti-human CD31 (clone WM59, catalog # 303139)
anti-human CD314 (NKG2D) (clone 1D11, catalog # 320837)
anti-human CD33 (clone P67.6, catalog # 366633)
anti-human CD335 (NKp46) (clone 9E2, catalog # 331941)
anti-human CD34 (clone 581, catalog # 343537)
anti-human CD38 (clone HIT2, catalog # 303543)
anti-human CD39 (clone A1, catalog # 328237)
anti-human CD4 (clone RPA-T4, catalog # 300567)
anti-human CD40 (clone 5C3, catalog # 334348)
anti-human CD44 (clone BJ18, catalog # 338827)
anti-human CD45 (clone HI30, catalog # 304068)
anti-human CD45RA (clone HI100, catalog # 304163)
anti-human CD45RO (clone UCHL1, catalog # 304259)
anti-human CD49f (clone GoH3, catalog # 313635)
anti-human CD5 (clone UCHT2, catalog # 300637)
anti-human CD56 (NCAM) (clone QA17A16, catalog # 392425)
anti-human CD57 (clone QA17A04, catalog # 393321)
anti-human CD62L (clone DREG-56, catalog # 304851)
anti-human CD69 (clone FN50, catalog # 310951)
anti-human CD70 (clone 113-16, catalog # 355119)
anti-human CD73 (clone AD2, catalog # 344031)

anti-human CD80 (clone 2D10, catalog # 305243)
anti-human CD86 (clone IT2.2, catalog # 305447)
anti-human CD8a (clone RPA-T8, catalog # 301071)
anti-human CD95 (clone DX2, catalog # 305651)
anti-human HLADR (clone L243, catalog # 307663)
anti-human KLRG1 (clone 2F1/KLRG1, catalog # 138433)
anti-human TCRab (clone IP26, catalog # 306743)
anti-human TCRgd (clone B1, catalog # 331231)
anti-human TIGIT (clone A15153G, catalog # 372729)
anti-human Tim3 (clone F38-2E2, catalog # 345049)

Immunohistochemistry antibodies:
anti-human HLA-A,B,C (clone EMR8-5, Abcam, catalog # ab70328, dilution 1:6000)
anti-human HLA-DR,DP,DQ (clone CR3/43-CR3/45, catalog # M0775, Dako, dilution 1:750)
anti-human SOX10 (clone EP268, catalog # 383R-16, Cell Marque, dilution 1:1500)

Immunofluorescence antibodies
anti-human CD4 (clone 4B12, Dako, catalog # M7310, dilution 1:150)
anti-human CD8 (clone C8/144B, Dako, catalog # M7103, dilution 1:100)
anti-human SOX10 (clone EP268, Cell Marque, catalog # 383R, dilution 1:20,000)

IP Antibodies:
anti-human HLA-DR,DP,DQ (unconjugated clone Cr3/43, Santa Cruz, catalog # SC-53302)

Validation

Antibodies for flow cytometry were validated and titrated by staining PHA-stimulated and unstimulated human PBMCs. Anti-mouse TCRbeta constant domain was validated and titrated on TCR-transduced versus non-transduced human T cells. Anti-human MCSP and Fibroblast antigens were validate and titrated on patient-derived fibroblast or melanoma cell lines. These antibodies were used to monitor the purity of patient-derived melanoma cell lines.

CITEseq antibodies were validated on PBMCs, that were submitted for single-cell sequencing.

IP antibody was validated by evaluating the enrichment of pan HLA-class II complexes in immunoprecipitation experiments.

IHC and IF antibodies were validated using melanoma controls.

Eukaryotic cell lines

Policy information about cell lines

Cell line source(s)

Melanoma cell lines were originated from all the patients included in the study (Pt-A, Pt-B, Pt-C, Pt-D).
Monoallelic HLA lines were available from previous studies [Abelin, 2017; Sarkizova 2020]

Authentication

All melanoma cell lines were validated with flow cytometry for the expression of melanoma markers (MCSP) or fibroblast antigen. Whole exome sequencing and bulk RNA sequencing confirmed identity between melanoma cell lines and parental tumors.

HLA expression on monoallelic HLA lines was verified by flow cytometry.

Mycoplasma contamination

Cell lines were tested negative for Mycoplasma contamination.

Commonly misidentified lines
(See ICLAC register)

No commonly misidentified cell lines were used.

Human research participants

Policy information about studies involving human research participants

Population characteristics

This study included 4 patients with the following charateristics:
-Pt-A (corresponding to Pt. 1 in [Hu, Leet, 2021]); sex: male; age: 26; primary tumor location: back; site of resected disease: axillary lymph node; Stage: IIIC(T3bN3M0); previous treatment (>6 months before biopsy collection): IFNa; source: Dana Farber Cancer Institute (Boston, MA, USA).

-Pt-B (corresponding to Pt. 3 in [Hu, Leet, 2021]);sex: female; age: 51; primary tumor location: left calf; site of resected disease: skin; Stage: IIIC(T3bN2cM0); previous treatment (>6 months before biopsy collection): none; source: Dana Farber Cancer Institute (Boston, MA, USA).

-Pt-C (corresponding to Pt. 6 in [Hu, Leet, 2021]);sex: male; age: 61; primary tumor location: chest; site of resected disease: lung; Stage: IVM1b(T2aNoM1b); previous treatment (>6 months before biopsy collection): IFNa; source: Dana Farber Cancer Institute (Boston, MA, USA).

-Pt-D (corresponding to Pt. 12 in [Hu, Leet, 2021]);sex: female; age: 63; primary tumor location: right forearm; site of resected disease: axillary lymph node; Stage: IIIC(T2aN1bM0); previous treatment (>6 months before biopsy collection): none; source: Dana Farber Cancer Institute (Boston, MA, USA).

	Characteristic of patients with melanoma analyzed in Fig 4 (correlation between tumor mutation burden and tumor HLA-class II expression) are summarized in Supplementary Table 8. We included all the patients with available tumor WES or RNAseq (to calculate tumor mutation burden) and HLA-class I and II IHC, from DFCI-Neovax cohort (Hu, 2021), MGH cohort [Sade-Feldma, 2019], checkmate064 cohort [Rodig, 2018] and checkmate038 cohort [Anagnostou, 2020]
Recruitment	We included in discovery cohort all patients enrolled in trial [Ott, 2017], with available pre-treatment tumor specimens viably frozen for single-cell experiments. To correlate tumor mutation burden and tumor HLA expression (Fig.4), we included all the patients with available tumor WES or RNAseq (to calculate tumor mutation burden) and HLA-class I and II IHC, from DFCI-Neovax cohort (Hu, 2021), MGH cohort [Sade-Feldma, 2019], checkmate064 cohort [Rodig, 2018] and checkmate038 cohort [Anagnostou, 2020] Patients Peripheral blood dynamics were studied on all the patients included in study [Sade-Feldma, 2019], treated at Massachusetts General Hospital (Boston, MA, USA) and with available blood specimens
Ethics oversight	This study was conducted in accordance with the Declaration of Helsinki. All the patients from whom specimens were obtained and analyzed (Supplementary Table 3 and 8) provided written informed consent for the collection of tissue samples for research and genomic profiling. Samples were obtained from tstudy subjects on IRB-approved protocols at DFCI.Dana Farber Cancer Institute (Boston, MA, USA) and Massachusetts General Hospital (Boston, MA, USA)

Note that full information on the approval of the study protocol must also be provided in the manuscript.

Clinical data

Policy information about clinical studies

All manuscripts should comply with the ICMJE guidelines for publication of clinical research and a completed CONSORT checklist must be included with all submissions.

Clinical trial registration	NCT01970358, NCT01783938 and NCT01621490
Study protocol	https://clinicaltrials.gov/ct2/show/NCT01970358 https://clinicaltrials.gov/ct2/show/NCT01783938 https://clinicaltrials.gov/ct2/show/NCT01621490
Data collection	NCT01970358 Enrollment: May 2014 to July 2016. Data collection: June 2014 to September 2019. NCT01783938 Enrollment: April 2013 to April 2015. Data collection: April 2013 to March 2021. I NCT01621490 Enrollment: September 2012 to September 2017. Data collection: September 2012 to March 2019. I For all the trials: blood and/or tumor samples were obtained in visit and/or during surgical procedures.
Outcomes	This study used data generated in clinical trials NCT01970358, NCT01783938 and NCT01621490. This study do not constitute a clinical trial by itself. The primary aim of such study was to correlate the number of coding tumor mutations and HLA expression of melanoma collected before treatment initiaion. The seconday aim was to evaluate post-treatment outcome (overall survival and progression-free survival) in relation to HLA-class II expression and tumor mutation burden of corresponding melanomas. Tumor mutation burden was assessed from WES or RNAseq, as described in Methods and Supplemetary Information sections. HLA-class I and II expression was assessed on SOX10+ melanoma cells by IHC stainings (see Methods and Supplemetary Information) Overall survival and progression free survival were evaluated at study completion, as reported in corresponding publications (NCT01970358: Hu, Nat Med 2020; NCT01783938: Rodig et al, Sci Transl Med 2018; NCT01621490: Anagnostou et al, Cell Rep Med 2020)

Flow Cytometry

Plots

Confirm that:

☒ The axis labels state the marker and fluorochrome used (e.g. CD4-FITC).

☒ The axis scales are clearly visible. Include numbers along axes only for bottom left plot of group (a 'group' is an analysis of identical markers).

☒ All plots are contour plots with outliers or pseudocolor plots.

☒ A numerical value for number of cells or percentage (with statistics) is provided.

Methodology

Sample preparation	Tumor samples were obtained immediately following surgery. The tissue was carefully minced manually, suspended in a solution of collagenase D (200 unit/mL) and DNAse I (20 unit/ml) (Roche Life Sciences), transferred to a sealable plastic bag and incubated with regular agitation in a Seward Stomacher Lab Blender for 30-60 min. After digestion, any remaining

clumps were removed and the single cell suspension was recovered, washed, and immediately frozen in aliquots and stored in vapor-phase liquid nitrogen until time of analysis. Heparinized blood samples were obtained from the same study subjects on IRB-approved protocols at DFCI or MGH. Patient peripheral blood mononuclear cells (PBMCs) were isolated by Ficoll/ Hypaque (GE healthcare) density-gradient centrifugation and cryopreserved with 10% dimethylsulfoxide (Sigma-Aldrich) in fetal bovine serum (FBS, Gibco, Thermofisher). Cells from patients were stored in vapor-phase liquid nitrogen until time of analysis.

Tumor or PBMC samples were thawed and then rested in RPMI containing 10% FBS and 1% penicillin/streptomycin for 4-6 hours. Subsequently, cells were filtered with a 100 mm cell-strain to remove debris, resuspended in fresh media and labeled with Live/Dead Zombie Aqua (BioLegend) for 10 min at 4°C, following by staining with antibody mixture for 20-30 min at 4°C.

For TCR antigenic specificity, cells were harvested after stimulation, washed twice and stained with antibody mixture for 20 min at room temperature.

Instrument

Cells were sorted on a BD Aria cell sorter (BD Biosciences) or were acquired on a high throughput sampler (HTS)-equipped Fortessa cytometer (BD Biosciences)

Software

FACSDiva (version 8.0.1) and FlowJo (version 10.3) were used to collect and analyze the flow cytometry data, respectively

Cell population abundance

Post-sort samples were analyzed for purity using the same FACS sorter. Using the same gating strategy , the purity of the samples was determined and calculated to be > 95%

Gating strategy

Before gating on fluorescence, live, single cells were gated using FSC-A and SSC-A (for intact cells) and FSC-W/ FSC-H (to ensure that only singlets were sorted). FACS gates were drawn to include only live single cells based on Zombie-Aqua negativity (Biolegend).

To sort tumor populations, further gates were drawn to identify CD3+CD45+, CD45+ CD3- or CD45- populations (for selected samples) or just viable cells (for selected samples). PBMCs were processed in parallel to isolate CD45+ CD3+ populations.

To sort PBMC fractions , viable lymhocytes were further identified as Zombie-Aqua - CD3+ cells. Gates were drewn on CD4+ CD8- cells and the followinf population were identified as depicted in Extended Data Fig. 5a: naïve cells (CD45RA+), memory cells (CD45RA-CD127+), effector cells (CD45RA- CD127- CD25-) and TReg cells (CD45RA-CD127-CD25bright).

For flowcytometry analysis of TCR transduction signal , gating strategy for CD8-(CD4+) T cells have been previously published (Oliveira et al, Nature 2021; Supplementary Information).

Strategies for analysis of dextramer + T cells or degranulating or cytokine producing cell are reported in Extended Data Fig.7.

☒ Tick this box to confirm that a figure exemplifying the gating strategy is provided in the Supplementary Information.